HIGH-TEMPERATURE ULTRASONIC MEASUREMENTS OF ROTATIONAL RELAXATION IN DIATOMIC MOLECULES

By

GARNETT LEE HILL

Bachelor of Science
Northwestern State College
Alva, Oklahoma
1960

Master of Science
Wichita State University
Wichita, Kansas
1962

Submitted to the faculty of the Graduate College
of the Oklahoma State University
in partial fulfillment of the requirements
for the degree of
DOCTOR OF PHILOSOPHY
May, 1968

OKLAHOMA
STATE UNIVERSITY
LIBRARY

OCT 25 1968

HIGH-TEMPERATURE ULTRASONIC MEASUREMENTS OF ROTATIONAL RELAXATION IN DIATOMIC MOLECULES

Thesis Approved:

Thomas S. Hunter
Thesis Adviser

Leon W. Schroeder

L. M. Raff

H. Harrington

E. E. Luke

N. Durham
Dean of the Graduate College

688384

ACKNOWLEDGMENTS

I wish to express my appreciation to Dr. T. G. Winter for his suggestions and direction throughout the course of this investigation.

Particular thanks is also extended to Dr. L. M. Raff for his valuable contributions to the interpretation of the data obtained in this investigation, Mr. W. Adkins for his advice and help in constructing the glassware, and Mr. E. Carnevale for technical information on equipment design.

Financial support administered through the Research Foundation and made available by the United States Army Research Office, Durham, North Carolina, is gratefully acknowledged.

TABLE OF CONTENTS

TABLE OF CONTENTS (Continued)

LIST OF TABLES

LIST OF FIGURES

LIST OF FIGURES (Continued)

CHAPTER I

INTRODUCTION

General Remarks

Ultrasonic absorption and velocity data can supply important information about the structure of matter and molecular processes. Failure of internal degrees of freedom within a molecule to stay in thermal equilibrium with the translational degrees of freedom causes velocity dispersion and absorption of sound in gases. The coupling of translational to internal energy is usually a relaxation process in which the internal energy reaches equilibrium exponentially with a time constant called the relaxation time. In a relaxation process, measurements of acoustic absorption or velocity are necessary over a large range of frequencies in order to understand the energy exchange mechanism. The important experimental information is the frequency of maximum absorption, height and shape of the absorption peak, and frequency and magnitude of the velocity dispersion. It is the vibrational and rotational relaxation processes which are of primary importance in acoustical investigations. Of these, the vibrational relaxations have been more widely investigated and are better understood. There is quite good agreement between theory and experiment for the vibrational degree of freedom in simple molecules.

Experimental measurements of the vibrational relaxation time have been determined for many gases over large temperature ranges by a variety of experimental methods. The temperature dependence of the vib-

rational relaxation time has been calculated classically and quantum mechanically for diatomic molecules and is in good agreement with experimental results. The most successful theory is that of Schwartz, Slawsky, and Herzfeld[1], who calculated transition probability using a quantum mechanical theory based on distorted wave techniques. The resulting expression contains the interaction potential, mass, etc., as parameters, all of which are obtained from other experiments; there are no adjustable parameters. This theory predicts the experimental values of the relaxation times within a factor of four for gases with vibrational relaxation times ranging from 10^{-1} to 10^{-8} seconds. This theory fails: (1) for large polyatomic molecules, (2) when the energy exchange is between rotation and vibration, and (3) where a permanent dipole moment leads to a preferred orientation upon collision. Nevertheless, by using parameters derived from spectroscopy and viscosity experiments, the vibrational relaxation time can be predicted for many diatomic molecules and a valid mathematical model of energy transfer exists. The same statement cannot be made for rotational relaxation.

Status of Rotational Relaxation Theory and Experiment

A satisfactory theory of rotational relaxation has proven more difficult for three principal reasons: (1) The perturbation methods successfully used for the case of vibrational relaxation are not valid for the large transition probabilities encountered in most rotational relaxations. (2) The acoustic data which has provided the principal experimental key to the understanding of vibrational relaxation is more difficult to interpret because if many rotational levels are occupied, each presumably has its own relaxation time, yet one can measure only

the over-all result. (3) Very little experimental data on rotational relaxation exists.

The principal quantum mechanical attacks on the problem of translational-rotational exchange have been made by Takayanagi[2] and Wang Chang and Uhlenbeck[3]. Other contributions are listed in Herzfeld and Litovitz[4]. The essential problem is that these calculations, depending upon perturbation theory, are not valid for most molecules because the transition probabilities are high.

Among the investigators who have predicted the temperature dependence of the rotational relaxation time, Berend and Benson[5] have carried out two-dimensional classical calculations and have obtained negative temperature coefficients for the rotational relaxation time. However, they suggest that a positive coefficient may be expected at elevated temperatures because the collision rate is decreasing as the temperature is increased for constant pressure. The problem has been solved classically in closed form with some simplifying assumptions by Parker[6], who was forced to choose a particularly simple interaction potential. He predicted that the rotational relaxation time should increase with temperature, but he predicts a shift which is considerably smaller than that observed. Raff[7] has suggested that positive temperature coefficients of the rotational relaxation time result from the fact the rotational transfer process is a many-level one, involving excitation rate constants which should decrease for higher rotational energy levels.

Purpose of Investigation and Discussion of Instrument

The purpose of this investigation was to examine the temperature dependence of the rotational relaxation of diatomic molecules. The tem-

peratures investigated ranged from room temperature to 1000°C, a region which had not been previously explored. It is apparent from the above discussion that there is a need for an instrument which can be used to measure the rotational relaxation time, as well as for data in the higher temperature range to overlap that obtained from shock tubes.

A diagram of the instrument used in this investigation is shown in Fig. 1. This new ultrasonic acoustical instrument was designed and constructed to measure the velocity and absorption of sound in gases at high temperature over a frequency range from .7 to 50 MHz/atm. A horizontal tube furnace heats the test gas, which flows continuously down a two-inch Vycor tube. Pulsed 1 MHz sound waves produced by lead zirconate transducers are conducted into the chamber through one-inch by twelve-inch fused quartz rods. The length of the sound path in the gas is adjusted with the two-inch travel micrometer attached to the right-hand quartz rod. The vacuum seals between the Vycor tube and the quartz rods are made from viton O-rings and teflon washers surrounded by a water-cooled jacket. Measurements made with this apparatus on non-relaxing argon were in agreement with the absorption and velocity measurements of other investigators[8].

The preparation and procedure used for taking ultrasonic velocity and absorption measurements are discussed in Appendix A. The design and assembly of the ultrasonic instrument are discussed in Appendix B. Appendix C gives the details on the preparation of the para-hydrogen used in this investigation. Information on the thermal-conductivity instrument used to analyze the para-hydrogen content is also presented. Chapter II includes definitions and a discussion of theory designed to aid in interpreting and understanding the data taken with this instru-

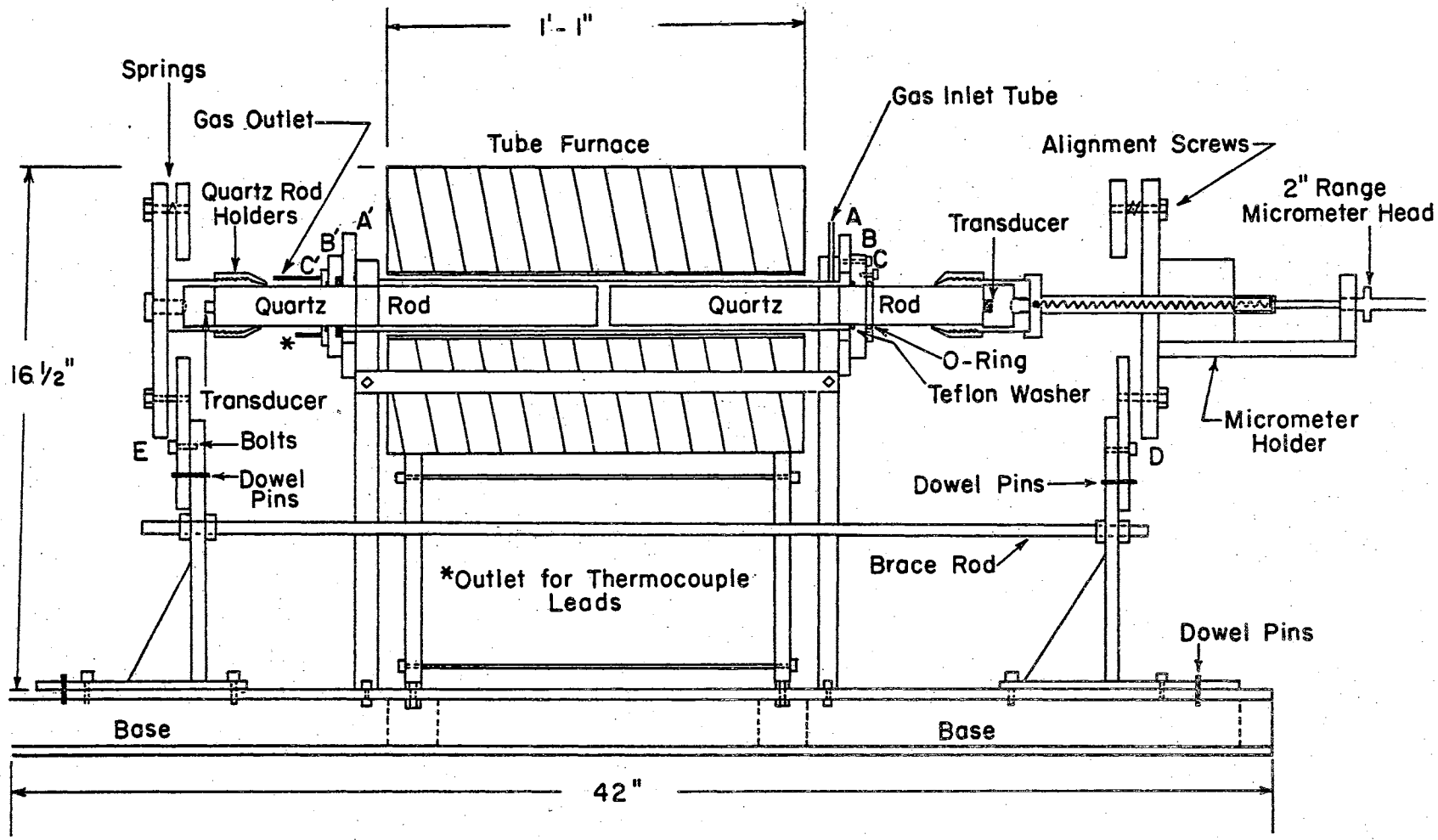

Figure 1. Instrument for Measuring Ultrasonic Velocity and Absorption

ment. Chapter III gives normal hydrogen, para-hydrogen, and deuterium absorption and dispersion data. In nitrogen and oxygen, the rotational energy levels are very closely spaced in comparison to hydrogen and deuterium, and the oxygen and nitrogen data is reported in Chapter IV. It has been found that the frequency of maximum absorption and the inflection point of the velocity dispersion curve always decrease with increasing temperature, and this leads to the remarkable conclusion that the rotational relaxation time increases with temperature! Chapter V discusses this and other results of this investigation.

CHAPTER II

DEFINITIONS AND THEORY

Relaxation Time and Collision Number Defined

If E is the momentary value of energy for an internal degree of freedom and $E(T_{tr})$ is the value it would have in equilibrium with the translational degree of freedom which is at a temperature of T_{tr}, then the relaxation time, τ, is defined by the following equation:

$$-\frac{dE}{dt} = \frac{1}{\tau}\left[E - E(T_{tr})\right] . \tag{2.1}$$

If there are only two energy levels (the two-state case), then only one relaxation time will describe the energy transfer process. However, in general, there will be a rate equation such as (2.1) for each possible transition. A simplification occurs for the harmonic oscillator where the energy levels are all evenly spaced, and one relaxation time constant will describe the rate of energy transfer to or from the entire degree of freedom[9]. The rate constants are different for the different states of the harmonic oscillator, but the relaxation times of the different transitions fit together to give a single relaxation time for the whole internal energy.

In general, the relaxation time can be obtained from the frequencies at which velocity dispersion and absorption occur. Experimentally it is easier to vary the pressure and thus the collision frequency of the gas than to work at different frequencies. At a given temperature

for an ideal gas, the velocity and absorption depend only on the ratio f/p and not on the individual values of sound frequency and pressure. If Z denotes the "collision number", which is the average number of collisions required to reduce the deficit of an internal energy to e^{-1} of its equilibrium value, then the collision number is equal to the product of the relaxation time and the collision frequency. The time between collisions, τ_c, is the reciprocal of the collision frequency, so that $Z = \tau/\tau_c$. For a gas near ideal conditions, $\tau_c \propto \frac{1}{p}$. Since the collision efficiency depends only on the kinematics, i.e., the relative velocity and distance of closest approach, of the colliding molecules and since the transfer of energy between translational and internal degrees of freedom takes place only in intermolecular collisions, then Z must be independent of pressure. Thus τp equals a constant and the combination of $(\omega\tau)$ which normally appears in all dispersion and absorption phenomenon may be increased by either increasing the frequency or decreasing the pressure.

Velocity of Sound in Gases

The low frequency value of the phase velocity of sound in monatomic gases is given by $V^2 = \frac{\gamma RT}{M}$, where R is the universal gas constant, (2.2) T the absolute temperature, and M the molecular weight. The ratio of specific heats, γ, can be written as

$$\gamma = C_p/C_v = (C_v + R)/C_v = 1 + R/C_v \tag{2.3}$$

for an ideal gas. The equation (2.2) then becomes

$$V^2 = \frac{RT}{M}\ (1 + R/C_v) \tag{2.4}$$

where $C_v = C_v$ (translation) = 3/2 R. This equation is valid provided the frequency of the sound wave is much less than the frequency between collisions of the molecules. When f/p is greater than 100 MHz and the frequency of the sound wave approaches the collision frequency of the molecules, translational dispersion occurs.

For diatomic gases at low frequency, equation (2.4) is still valid, but C_v now may also contain contributions from rotation and vibration, i.e.,

$$C_v = C_v \text{ (tra.)} + C_v \text{ (rot.)} + C_v \text{ (vib.)} \tag{2.5}$$

When the frequency-to-pressure ratio is increased, the vibrational contribution to the specific heat may be eliminated because the period of the wave becomes shorter than the vibrational time constant, and this causes an increase in the sound velocity. As the frequency-to-pressure ratio is increased further, the rotational contribution to the specific heat may leave, causing rotational velocity dispersion to occur before translational dispersion disseminates the energy of the sound wave.

Herzfeld and Litovitz derive a general expression for the velocity of any frequency sound wave by defining "effective specific heats" and using the Stokes-Navier equation. The Stokes-Navier equation results from applying the continuity equation, Newton's second law for the motion of matter, the equation of state for the gas, and stress expressions which include viscous terms. The effective specific heat is defined as

$$(C_v)_{\text{eff}} = C_v + C' \frac{dT'}{dT_{tr}} \tag{2.6}$$

where C_v is the specific heat of the external degrees of freedom and C' is the specific heat of the relaxing internal degrees of freedom. The derivative of temperature of the internal degree of freedom with respect to the external degrees of freedom is $\frac{dT'}{dT_{tr}}$. When $\frac{dT'}{dT_{tr}} \approx$ unity (low frequency sound waves), the internal specific heat participates to give an effective specific heat which is equal to the static value of the specific heat. By using equation (2.1) and assuming the sound waves cause periodic variations in temperature proportional to $e^{i\omega\tau}$, then $\frac{dT'}{dT_{tr}}$ becomes

$$\frac{dT'}{dT_{tr}} = \frac{1}{1 + i\omega\tau} \tag{2.7}$$

Thus, by introducing a phase lag between external and internal degrees of freedom through effective specific heats and using the Stokes-Navier equation, the velocity as a function of the sound frequency can be derived by making the approximation that the classical and molecular absorptions are additive. (Classical absorption is derived in the next section.) The velocity is given by

$$V^2 = V_o^2 \left[1 + \frac{(C_p - C_v)C'}{C_p(C_v - C')} \cdot \frac{\left(2\pi \left[\frac{C_p - C'}{C_p}\right]\tau \frac{f}{p}\right)^2}{1 + \left(2\pi \left[\frac{C_p - C'}{C_p}\right]\tau \frac{f}{p}\right)^2} \right] \tag{2.8}$$

where V_o is the low frequency sound velocity, f the frequency, p the pressure, and the subscripts p and v on the specific heats are for constant pressure and volume respectively. The shape of this single relax-

ation dispersion is shown in the top solid curve in Fig. 3. Equation (2.8) shows that a large relaxing specific heat produces a large velocity dispersion, and a long relaxation time requires low frequencies in order to observe the dispersion region. The inflection point in the velocity dispersion curve appears where $(2\pi f) \approx \frac{1}{\tau}$.

The correction of sound velocity measurements to an ideal gas state can be computed in terms of the second virial coefficient[10]. The second virial coefficient can be measured experimentally or calculated from the critical temperature and pressure of the gases. The corrections to the sound velocity are negligible for the gases in this investigation.

Absorption of Sound in Gases

The important absorption losses for the gases in this investigation are due to molecular processes, thermal conductivity, and viscosity.

In molecular absorption, the energy is stored internally and is released to the external degrees of freedom out of phase because of a time lag in the transfer of energy between internal and external degrees of freedom. As a sound wave traverses the gas, the compression regions cause an increase in the translational energy of the molecules. If translational and rotational coupling occurs, energy is transferred to rotational energy of the molecules during the compression half-cycle. If a time lag occurs in the transfer of this energy, the energy does not revert to translational energy until the sound wave is in the decompression cycle. The energy is then out of phase and the height of the pressure peaks and depth of the troughs of the sound wave decreased. Energy is then removed from the ordered motion of the sound wave and absorption occurs.

By using the same methods and assumptions as those used to derive the velocity dispersion, but taking the imaginary part of the expression, the molecular absorption times the wavelength becomes:

$$\alpha_{mol}\lambda = \frac{V^2}{V_o^2}\left[\frac{\pi (C_p - C_v)C'}{C_v(C_p - C')} \cdot \frac{\frac{(C_p - C')}{C_p} 2\pi \frac{f}{p}\tau}{1 + \left[\frac{(C_p - C')}{C_p} 2\pi \frac{f}{p}\tau\right]^2}\right] \qquad (2.9)$$

The shape of this absorption curve is shown by the lower solid curve in Fig. 3. Equation (2.9) shows that a large relaxing specific heat increases the height of the absorption peak, and a long relaxation time requires low frequencies in order to observe the absorption region. The peak of the absorption curve occurs where $(2\pi f)\approx\frac{1}{\tau}$. The theoretical absorption and dispersion formulas for multiple relaxation in series and parallel have also been developed by Herzfeld and Litovitz. A 7040 computer program has been written for a double relaxation process in parallel. This program is used to calculate the theoretical molecular absorption and dispersion of a single relaxation process by setting one time constant and one relaxing specific heat, C', equal to zero. By choosing the relaxation time in this program, the dispersion and absorption can be fitted to the experimental data. The relaxing specific heat is usually known from statistical mechanics or spectroscopic data. If it is not known, it can be treated as unknown and determined from the magnitude of the dispersion or height of the absorption peak in a single relaxation process.

In the case of absorption due to heat conduction, the energy flows

from the high-temperature region of the compressions to the low-temperature region of decompressions. An absorption of sound energy due to viscosity arises because the pressure of a gas depends on the rate of change of the density of the gas. The absorption of sound due to thermal conductivity and viscosity is usually called classical absorption. For an ideal gas, the classical absorption was derived by Stokes, Kirchoff, and Langevin[11], and is given by

$$\alpha_{cl}\lambda = \frac{2\pi^2}{\gamma}\left[\frac{4}{3}n + \frac{(\gamma - 1)}{C_p}K\right]\left(\frac{f}{p}\right) \qquad (2.10)$$

where n is the viscosity and K is the conductivity. This expression for the classical absorption in monatomic and diatomic gases is a good approximation to 100 MHz/atm. Also, for frequencies below 100 MHz, the approximation is usually made that the classical absorption and molecular absorption are additive, i.e.

$$\alpha_{exp}\lambda = \alpha_{cl}\lambda + \alpha_{mol}\lambda \qquad (2.11)$$

where α_{exp} is the experimental absorption and α_{mol} is the molecular absorption.

A rather simple formula has been derived by Herzfeld for obtaining the rotational collision number from the experimental absorption. Several investigators have used

$$\frac{\alpha_{exp}}{\alpha_{cl}} = 1 + 0.067Z_r \qquad (2.12)$$

to obtain the rotational collision number when only the low frequency portion of the acoustical absorption can be obtained. Unfortunately this equation is valid only for independent parallel relaxation process-

es, and it is probably a crude approximation to apply this formula to a multilevel rotational system. Also, small errors in the experimental absorption result in large errors in the rotational collision number.

General Discussion of Diatomic Rotational Systems

For diatomic molecules, the translational energy is coupled to both rotational and vibrational energy. However, the following discussion will show that for hydrogen and deuterium, as well as for oxygen and nitrogen, dispersion and absorption due to vibration do not appear. The characteristic temperatures of vibration for hydrogen and deuterium are $5958^{\circ}K$ and $4211^{\circ}K$ respectively, and for temperatures below $1000^{\circ}C$ the vibrational specific heat is so low that its contribution to absorption can be neglected and any absorption above the classical must be due to the rotational relaxation[12]. The characteristic temperatures of vibration for oxygen and nitrogen are $2228^{\circ}K$ and $3336^{\circ}K$ respectively, and give a vibrational specific heat contribution at the higher temperatures of this experiment. However, the relaxation times of these gases have been measured and are approximately 10^{-3} sec[13]. The absorption maximum due to a relaxation time of 10^{-3} sec/atm occurs at a frequency around 250 cycles/sec, and the absorption would be negligible at the frequencies of this experiment. The rotational relaxation time constant is approximately 10^{-8} sec. Thus, in the frequency range from 1 to 100 MHz, the vibrational relaxation does not significantly affect the rotational relaxation for hydrogen, deuterium, nitrogen, or oxygen. The important molecular process then is coupling of translational energy to the internal degree of rotation.

Almost all previous experiments have shown that the relaxation time

always decreases with rising temperature. In this investigation it is shown for the first time, and shown conclusively, that the rotational relaxation time appears to increase with temperature. Interpretation of rotational relaxation dispersion and absorption data is complex because rotational energy levels are not equally spaced and the return to equilibrium is not exponential with a single time constant, but the result of many transitions with different time constants. A discussion of rotational energy levels for these diatomic molecules will aid in understanding why the experimental rotational relaxation time appears to increase with temperature. A qualitative argument will be presented in Chapter V, which suggests an explanation for why the relaxation time should increase with temperature and why approximate single relaxation dispersion and absorption curves should be observed for molecules with small rotational characteristic temperatures.

Molecules which behave as rigid rotors have an energy spectrum given by

$$E_j = j(j + 1)k\theta_r \qquad (2.13)$$

where $\theta_r = h^2/8\pi^2 Ik$, k is Boltzmann's constant, h is Plank's constant, I is the moment of inertia, and θ_r is the characteristic temperature of rotation.

In hydrogen and deuterium, the small value of the moment of inertia produces a large energy-level spacing. θ_r equals 84.8°K in hydrogen and 42.6°K in deuterium. Two modifications which depend on the total nuclear spin occur in these homonuclear molecules. In para-hydrogen, only even rotational energy levels of j = 0, 2, 4, - - - are allowed, and in ortho-hydrogen only the odd rotational states are allowed. Trans-

itions between the two modifications are forbidden and are only obtained by means of a catalyst. This has several consequences. First, ortho- and para-hydrogen can be treated as two distinct gases and second, the energy changes are larger because only transitions with $\Delta j = 2$ are allowed. In Fig. 2, the rotational energy levels are plotted where $kT = E_j = j(j + 1)k\theta_r$, or $T = j(j + 1)\theta_r$. This figure shows that for temperatures above room temperature, the corresponding quantum number is large for nitrogen and oxygen. Examination of the Maxwell Boltzmann distribution also shows that many levels are populated at high temperature. For hydrogen and deuterium, the number of possible transitions in a collision is small, and only a few levels are sufficiently populated to make a contribution to the specific heat, while for nitrogen and oxygen many levels are occupied and many different transitions presumably occur.

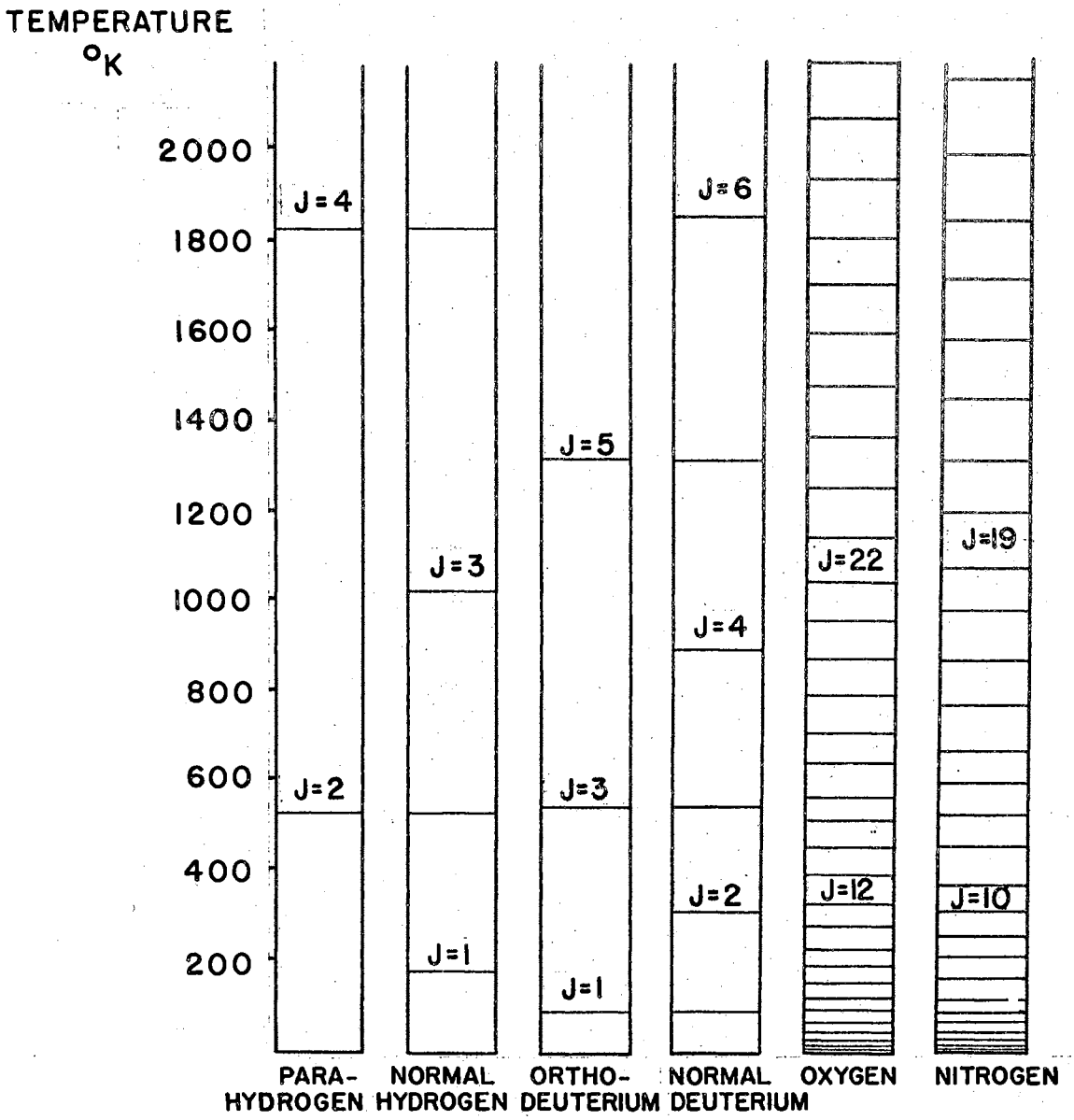

Figure 2. Rotational States of Hydrogen, Nitrogen, and Oxygen

CHAPTER III

NORMAL HYDROGEN, PARA-HYDROGEN, AND DEUTERIUM

Previous Low-Temperature Investigations

A. Van Itterbeek and co-workers[14] were the first to observe an excess absorption in hydrogen from 10-25 times the classical absorption and associated this excess absorption with the rotational degree of freedom. Others had sought this[15], but their work was not done at a sufficiently high ratio of frequency to pressure. Later the existence of this relaxation for the rotational energy was proven by dispersion measurements made by E. S. Stewart[16], whose room-temperature measurements indicate that a single relaxation is not strictly applicable to normal hydrogen. Room-temperature measurements performed by Rhodes[17] on pure para-hydrogen and normal hydrogen also indicate the possible existence of multiple relaxations. From velocity measurements on pure para-hydrogen, Rhodes also observed the inflection point to shift to higher f/p as the temperature increased from 197.1 to 298.4°K. The room-temperature measurements of Rhodes have been confirmed by Geide[18].

C. G. Sluijter, H. F. P. Knapp, and J. J. M. Beenakker[19] have measured the sound absorptions of hydrogen isotopes at 77, 90, and 293°K. For para- and ortho-hydrogen at 77 and 90°K, an absorption curve was found which could be fitted with the theoretical curve of a single-relaxation-time process. The relaxation time could be determined uniquely and a slight decrease was observed with increasing temperature. This is

in agreement with the single-relaxation dispersion measurement of Rhodes. The absorption measurements of Sluijter on ortho-deuterium show very little change over the temperature range from 77 to 293°K.

Experimental Data

Experimental velocity and absorption data are presented below for normal hydrogen, para-hydrogen, and deuterium. For normal hydrogen, Figs. 3, 4, and 5 show plots of $\alpha_{mol}\lambda$, the measured absorption minus the classical absorption times the wavelength, and the velocity squared versus f/p in MHz/atm. The classical absorption in normal and para-hydrogen has been calculated by equation (2.10) using thermodynamic data taken from reference 20, with the high-temperature values obtained by extrapolation. The thermodynamic data for deuterium was obtained from hydrogen data by the methods suggested in reference 21. The probable numerical error in $\alpha_{mol}\lambda$ is shown in Fig. 3 for two experimental points. The solid curves shown in the figures displaying the data have been drawn from single-relaxation theory to best fit both velocity and absorption data. The normal hydrogen and deuterium were used as received from the manufacturer without further treatment to increase purity. The para-hydrogen was prepared as discussed in Appendix C.

Normal Hydrogen

The hydrogen used was obtained from the Matheson Company, and mass spectrometer analysis showed its purity to exceed 99.997%. Fig. 3 shows room-temperature data which coincides with Stewart's findings, and agrees closely with single-relaxation theory indicated by the solid curves. A single-relaxation curve with a slightly longer relaxation

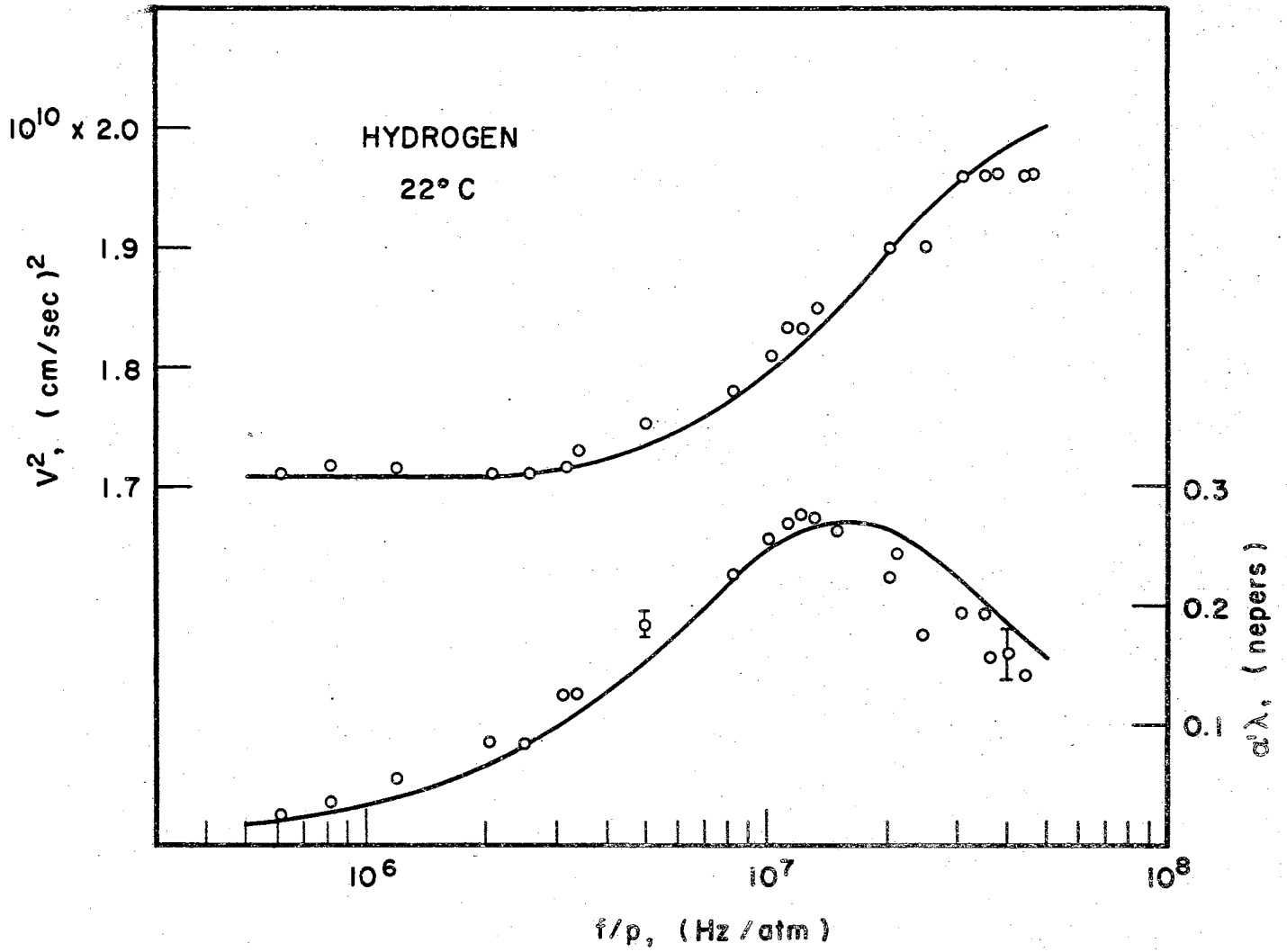

Figure 3. Dispersion and Absorption in Hydrogen, 22°C

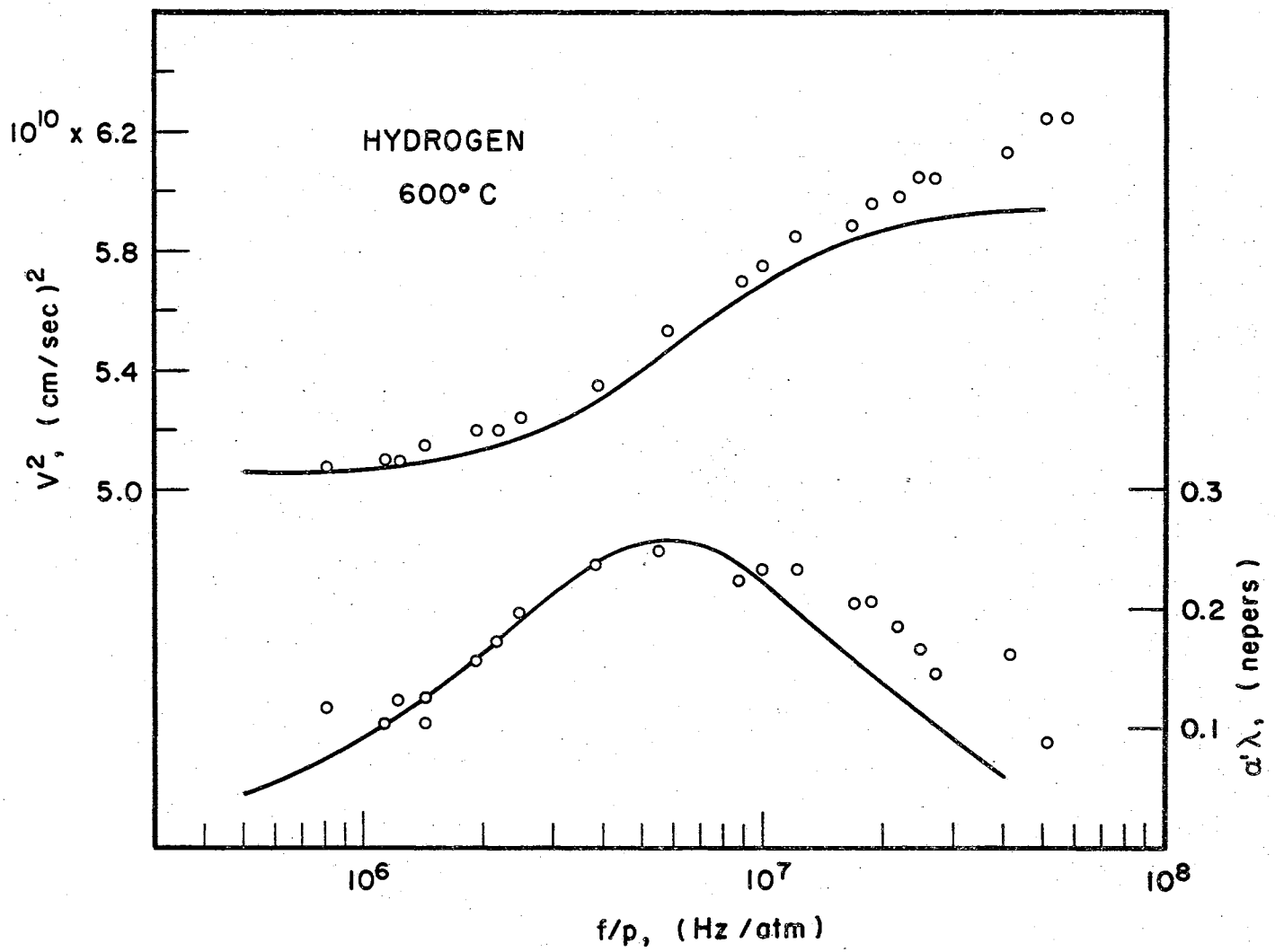

Figure 4. Dispersion and Absorption in Hydrogen, 600°C

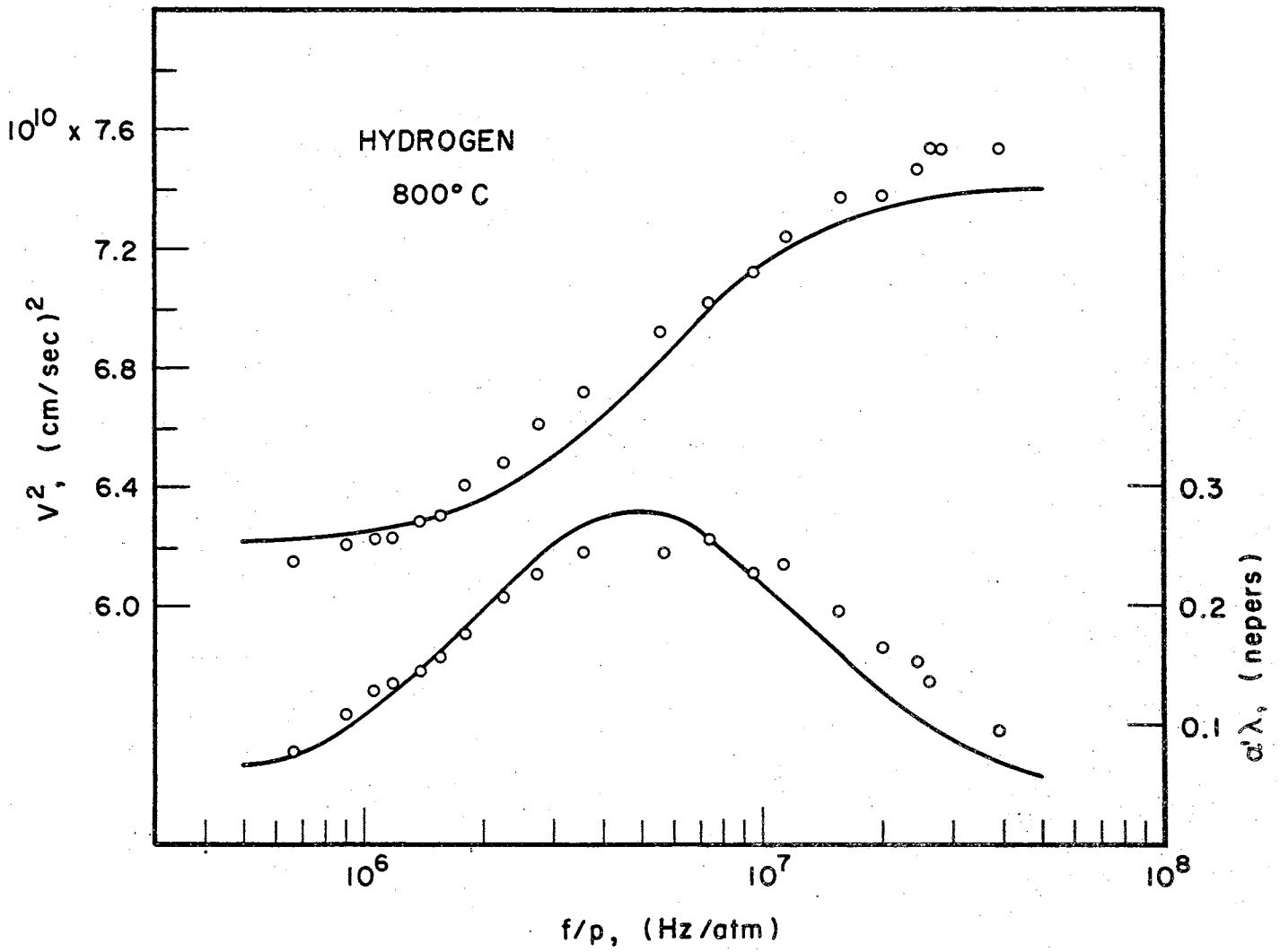

Figure 5. Dispersion and Absorption in Hydrogen, 800°C

time will give a better fit to the absorption data; however, this relaxation time does not fit the velocity dispersion data as well as the one shown in Fig. 3. Since normal hydrogen is in effect a mixture of two different gases, an approximation of a double relaxation in parallel can be made at room temperature. By assuming a double-relaxation process in parallel with relaxation times of $\tau_{02} = 1.3 \times 10^{-8}$ and $\tau_{13} = 1.9 \times 10^{-8}$ sec, a good fit to both the velocity and absorption data can be obtained. The relaxation time τ_{02} is the time associated with excitations in para-hydrogen from its ground state to the first excited rotational energy level, and τ_{13} is the relaxation time associated with excitations in ortho-hydrogen from its ground state to its first excited energy level. In this calculation, the specific heats were weighted by 75% ortho- and 25% para-hydrogen. A Cole[22] plot of this data is a semicircle with the center on the horizontal axis, indicating nearly a single-relaxation process. The peak of the absorption curve appears at 13 MHz/atm, which is also the inflection point of the velocity dispersion curve.

Figs. 4 and 5 show the same data for hydrogen at 600 and 800°C. The dispersion shown at 800°C is the largest ever reported, more than 275 m/sec. The most important feature is the shift of the absorption peak and the dispersion inflection point from 13 MHz/atm at 22°C to 5 MHz/atm at 800°C. The single-relaxation curves no longer describe the experimental points; there is a broadening of the absorption peak which is characteristic of multiple relaxations. Multiple relaxation is shown more clearly in Fig. 6, which is a Cole plot of the 800°C data. The vertical shift of the circle's center from the horizontal axis indicates that a single relaxation approximation is no longer valid.

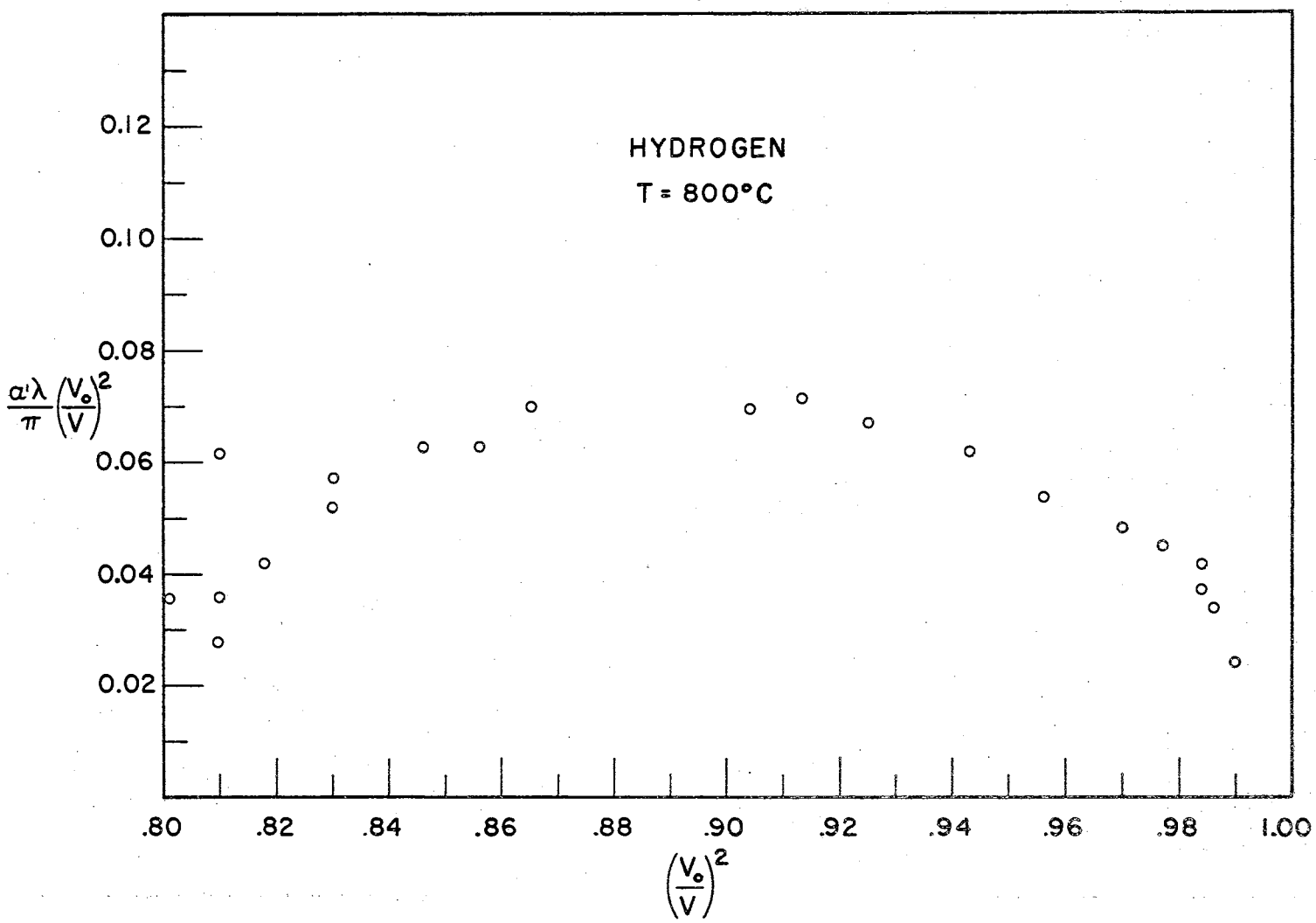

Figure 6. Cole Plot of Dispersion and Absorption in Hydrogen, 800°C

Para-Hydrogen

Ultra-high purity normal hydrogen from the Matheson Company was passed over a catlyst at 20°K to obtain the para-hydrogen. Mass spectrometric analysis showed the following impurities in the high purity hydrogen: oxygen, less than 1 part per million; nitrogen, less than 5 parts per million; and total hydrocarbons, less than .2 parts per million.

Figs. 7, 8, and 9 show the molecular absorption times the wavelength and the velocity dispersion in 99% para-hydrogen at 25°C, 91% para-hydrogen at 300°C, and 82% para-hydrogen at 500°C. The tests for the para-hydrogen content of the gas were made on the gas emerging from the tube furnace. There was no detectable conversion at room temperature, but unfortunately the percentage of para-hydrogen dropped with increasing temperature. Dispersion and absorption measurements were not made at 800°C where the composition was only 50% para-hydrogen. This conversion was apparently due to the energetic collisions or catalytic action of the quartz rods or Vycor tube.

Figs. 7, 8, and 9 show that the absorption and dispersion of para-hydrogen are nearly identical with normal hydrogen. Again the equilibrium time appears to be increasing with increasing temperature. The indistinguishableness of the absorption is shown more clearly by Figs. 10 and 11, where the experimental absorption times the wavelength vs f/p has been plotted for normal and para-hydrogen at 25 and 300°C. Geide has obtained similar results at room temperature; however, his para-hydrogen absorption is slightly higher than the normal hydrogen. The velocity dispersion in normal and para-hydrogen has also been plotted in Figs. 11 and 12. The shape of the dispersion curves appears in-

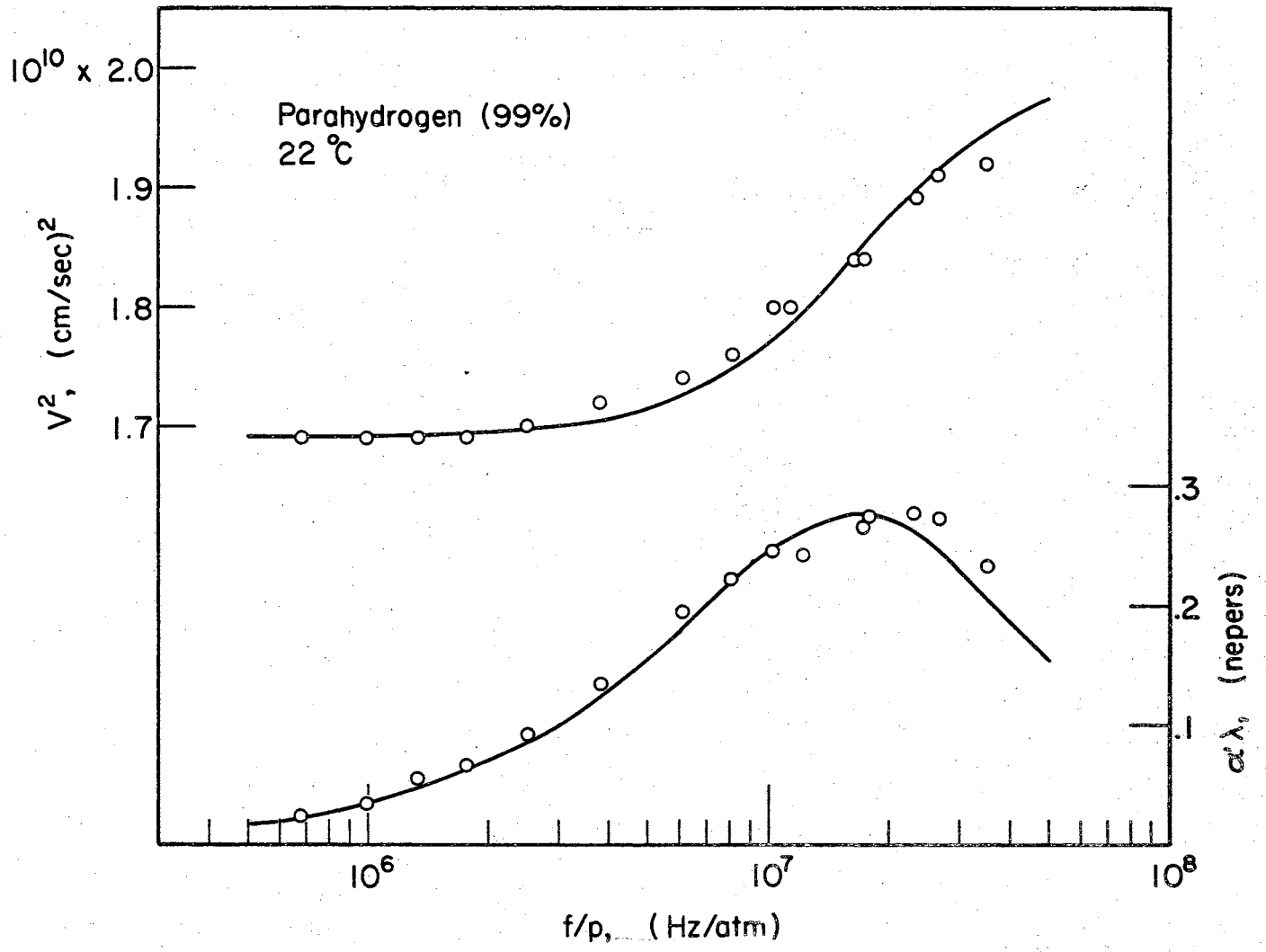

Figure 7. Dispersion and Absorption in Para-Hydrogen, 22°C

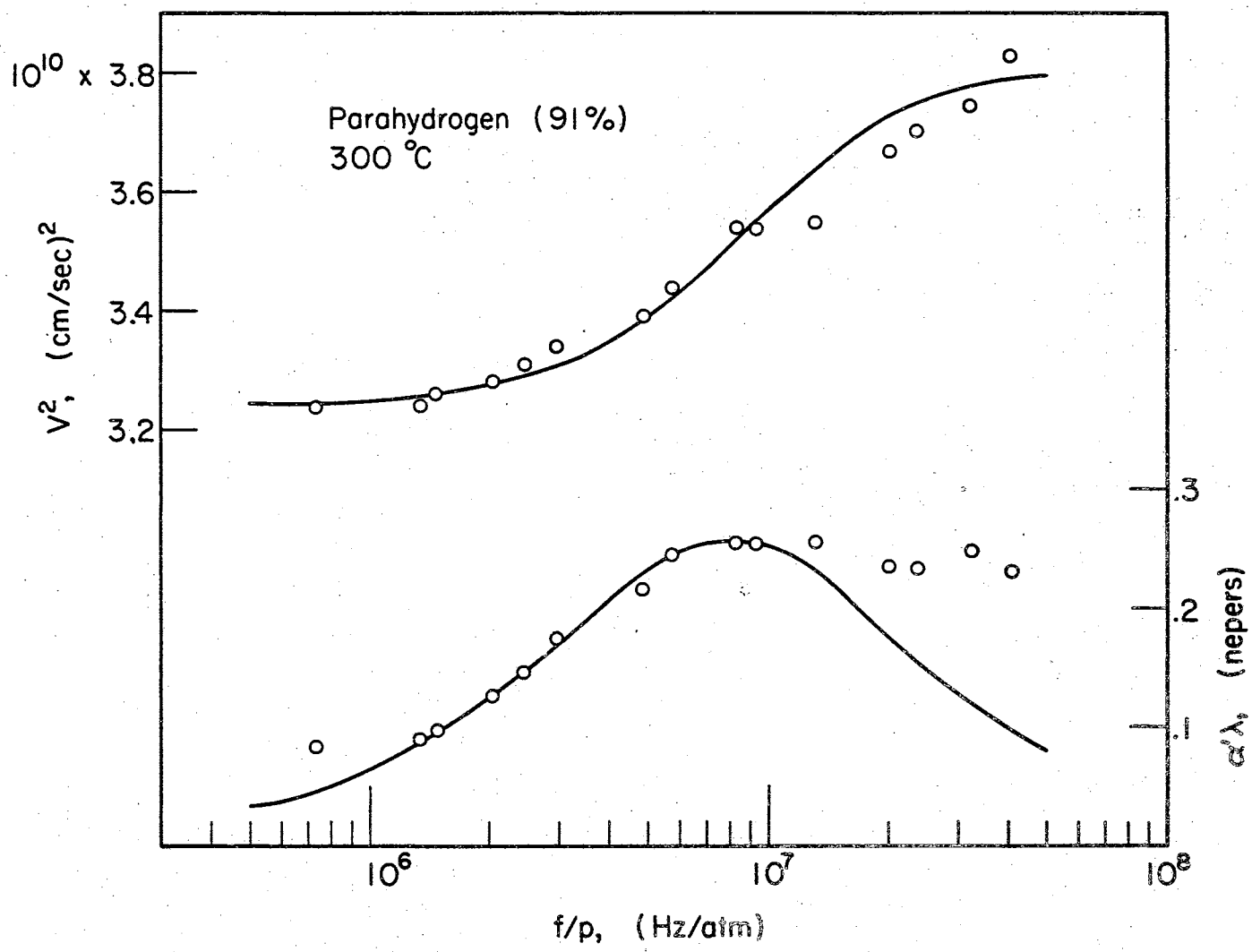

Figure 8. Dispersion and Absorption in Para-Hydrogen, 300°C

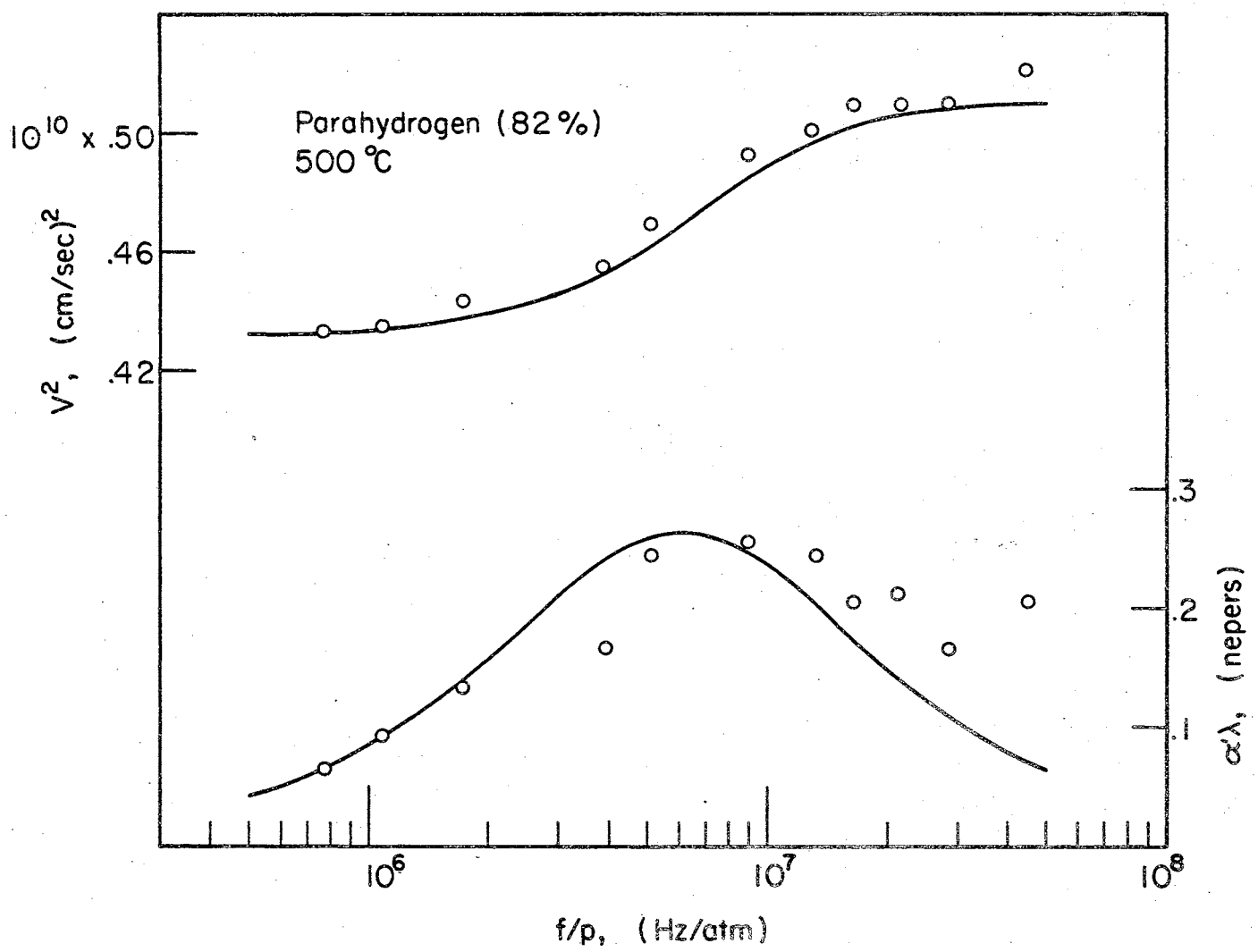

Figure 9. Dispersion and Absorption in Para-Hydrogen, 500°C

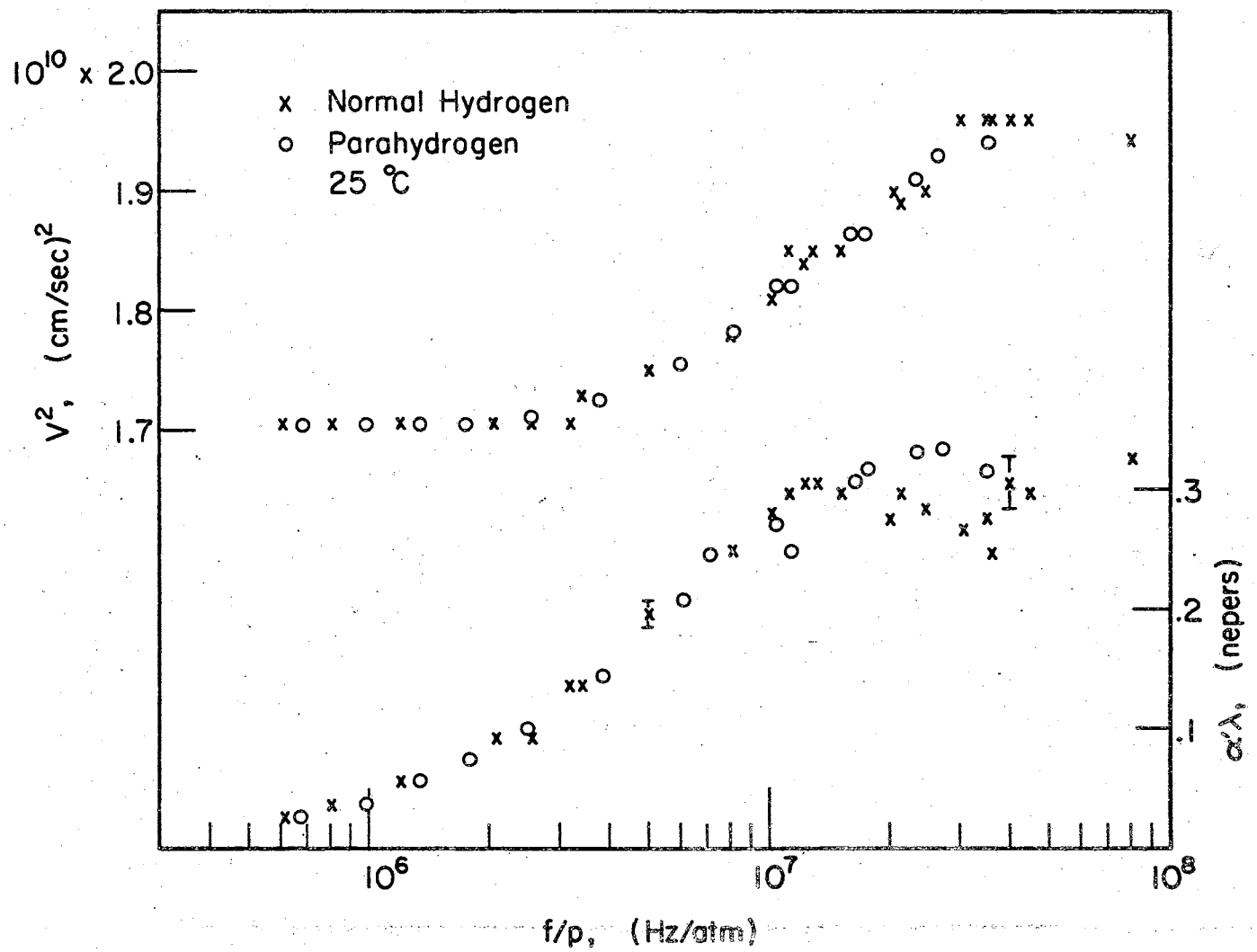

Figure 10. Dispersion and Absorption in Normal and Para-Hydrogen, 25°C

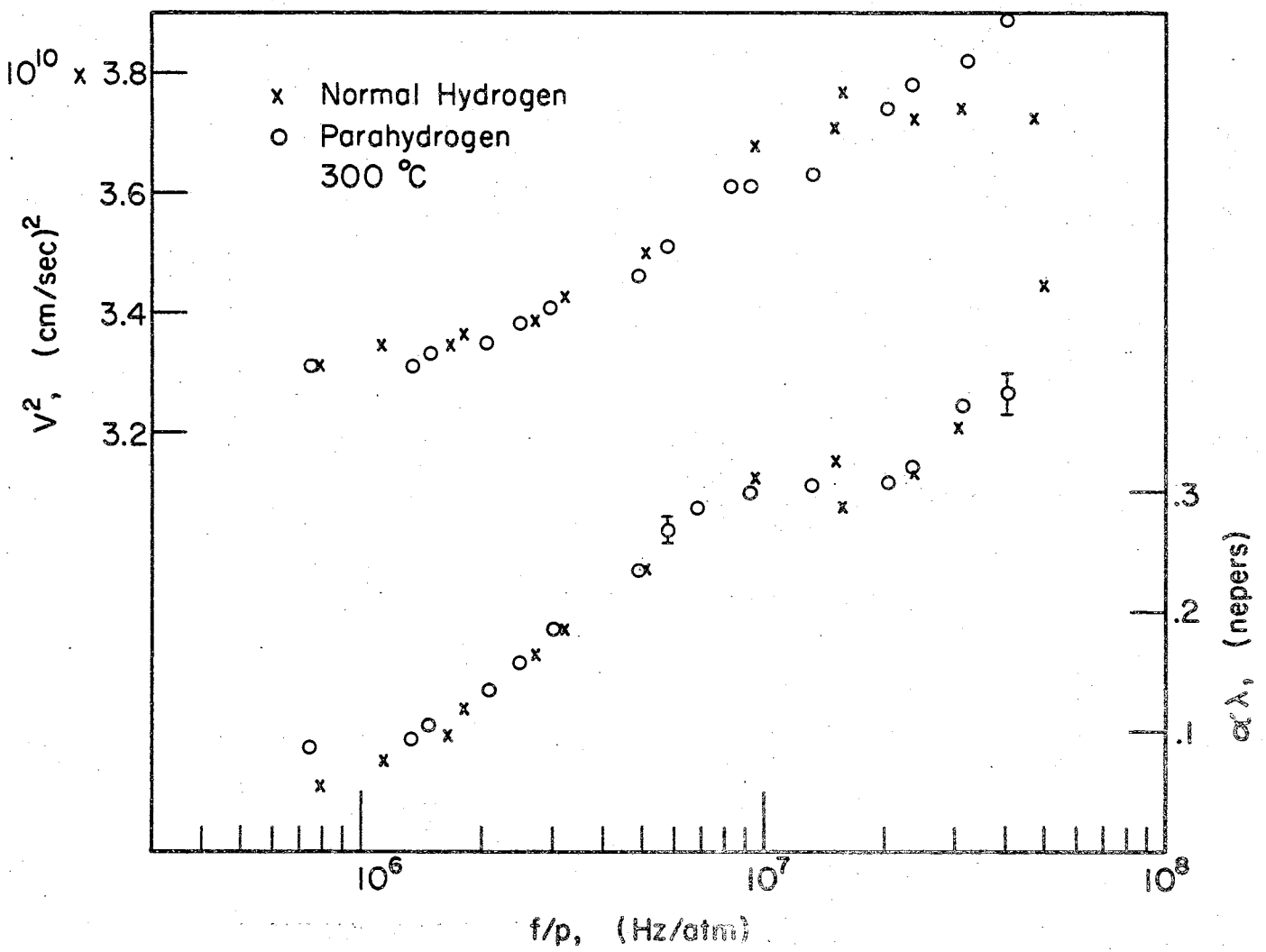

Figure 11. Dispersion and Absorption in Normal and Para-Hydrogen, 300°C

distinguishable. The low-frequency velocity of the para-hydrogen has been adjusted slightly so it will correspond to that of normal hydrogen. This was apparently necessary because of a change in the calibration of the thermocouple used to measure the temperature of the gas.

Deuterium

The deuterium used was also from the Matheson Company, and mass spectrometric analysis showed the following principal impurities: H. D. atoms - 2%, hydrogen - .07%, oxygen - 41 parts per million, and nitrogen - 350 parts per million. Figs. 12, 13, and 14 show the absorption and dispersion at 22, 500, and 800°C. Both the absorption and dispersion at room temperature are in good agreement with Stewart's findings. Figs. 12 and 14 also show that the absorption peak and dispersion inflection point shift from 17 MHz/atm at 22°C to 4 MHz/atm at 800°C, a larger shift than for hydrogen. Again, the high-temperature absorption peak is broader than a single-relaxation absorption peak.

Discussion of Results

Previous investigations of the rotational relaxation in the temperature range from 77°K to room temperature show conclusively that the relaxation time in ortho- and para-hydrogen decreases as the temperature increases. A single-relaxation-time process was observed and could be correlated with a definite excitation between known energy levels.

Data obtained in this investigation shows multiple relaxations become more apparent in hydrogen as the temperature increases from room temperature to 800°C. In normal hydrogen, para-hydrogen, and deuterium, the inflection point in the velocity dispersion curve and the peak of

the absorption curve shift to lower f/p as the temperature increases. This shift to lower f/p occurs primarily because higher energy levels are contributing to the rotational specific heat. Thus the apparent relaxation time corresponding to the high-temperature data does not correspond to the same rotational energy level transitions as it does for the low-temperature data.

In all of these gases, the magnitude of the velocity dispersion becomes larger as the temperature increases. In hydrogen the dispersion ranges from 90 m/sec at room temperature to over 275 m/sec at 800°C. Other conclusions from the data presented in this chapter are that the acoustic data of the para-hydrogen corresponds very closely to the normal hydrogen at 22, 300, and 500°C, and the inflection point and absorption peak shift slightly more for deuterium than for normal hydrogen over the total temperature range.

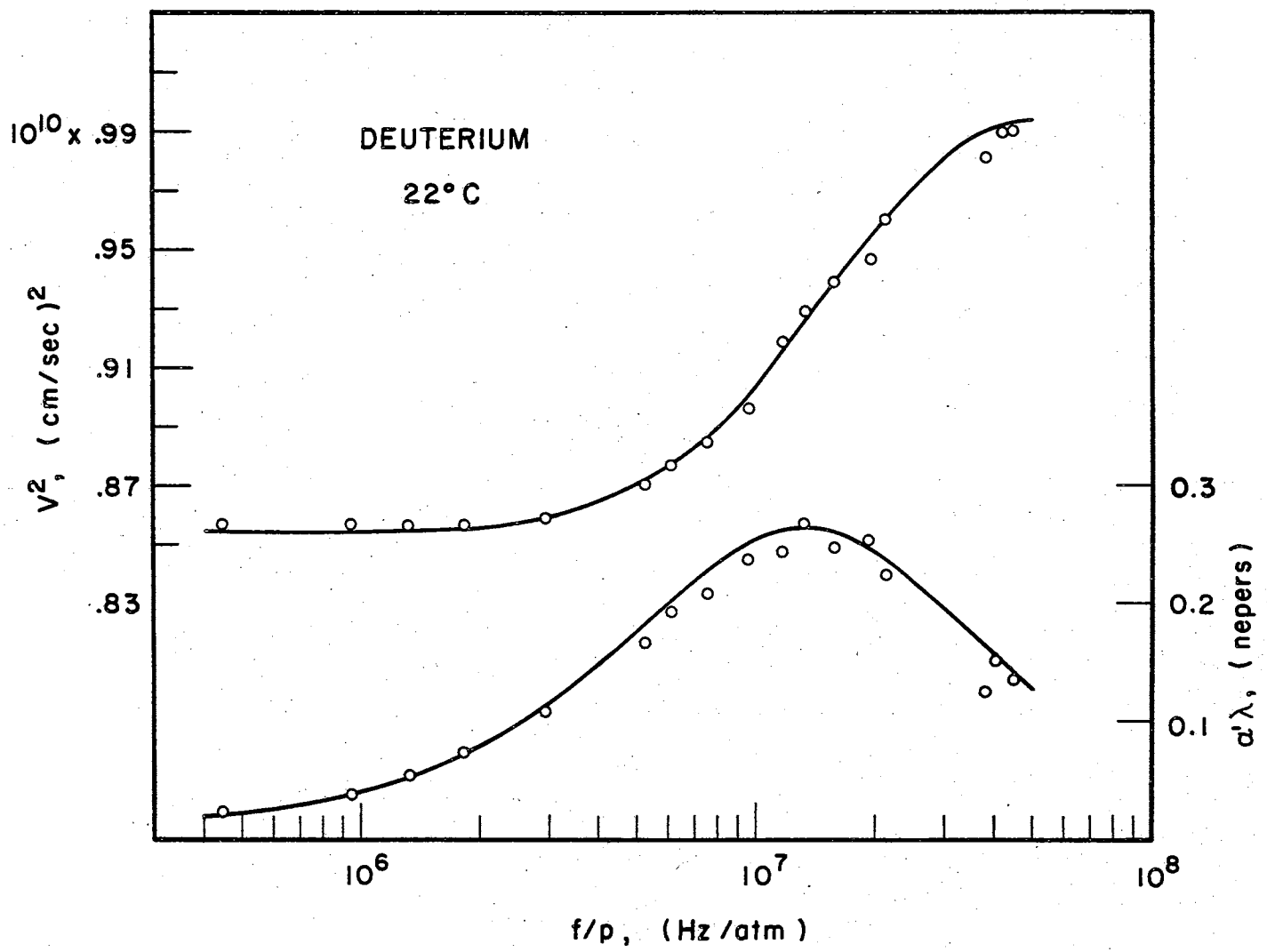

Figure 12. Dispersion and Absorption in Deuterium, 22°C

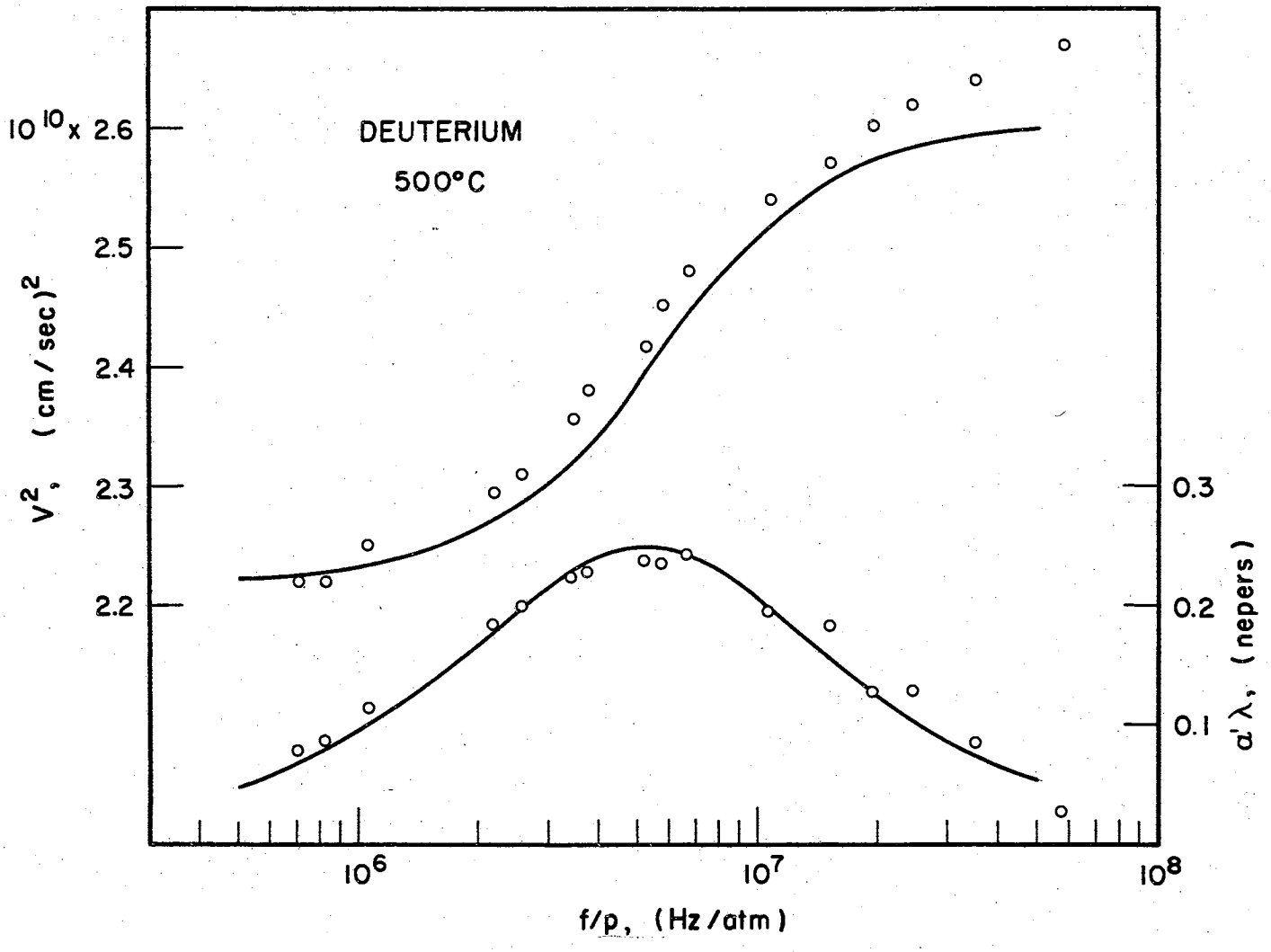

Figure 13. Dispersion and Absorption in Deuterium, 500°C

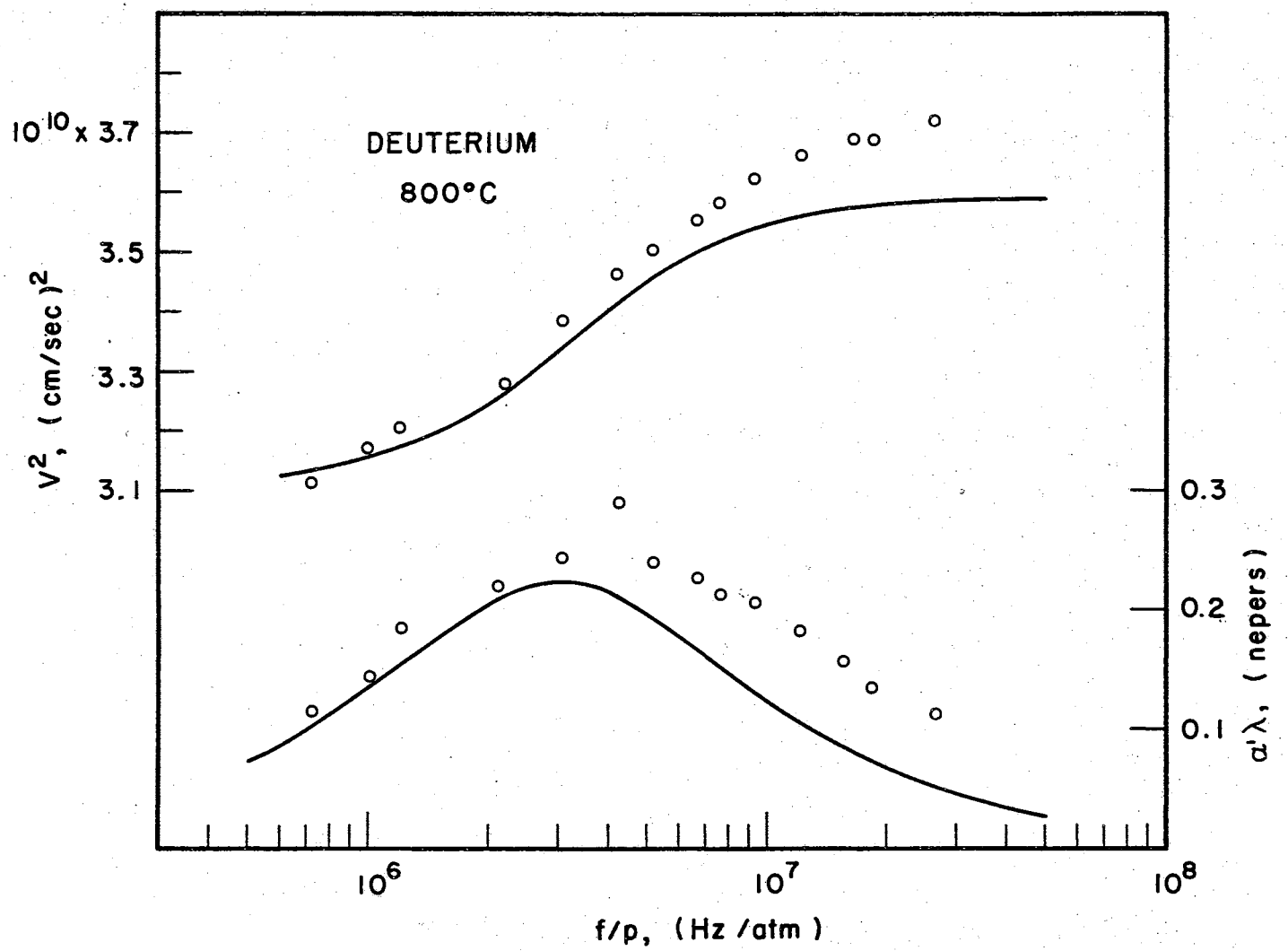

Figure 14. Dispersion and Absorption in Deuterium, 800°C

CHAPTER IV

NITROGEN AND OXYGEN

Previous Room Temperature Investigations

Since the rotational characteristic temperatures of nitrogen and oxygen are small compared to those of hydrogen and deuterium, the molecules of nitrogen and oxygen represent quite different rotational systems for acoustical investigation.

Robert A. Boyer[23] has measured the ultrasonic velocity extending into the translational dispersion region for nitrogen and oxygen at room temperature. He observed an increase in velocity of 16 and 20% for nitrogen and oxygen respectively when the frequency-to-pressure ratio ranged from 9 to 37 MHz/atm. Alfred J. Zmuda[24] found a room-temperature dispersion of 10 m/sec for nitrogen when the frequency-to-pressure ratio ranged from 3 to 114 MHz/atm. He also found α_{exp}/α_{cl} is approximately 1.4 in fair agreement with W. Tempest and H. D. Parbrook[25]. Zmuda has estimated the rotational relaxation time from the lower portion of the absorption curve to be 1.2×10^{-9} sec. This is in approximate agreement with Wayland Griffith's[26] measurements obtained by a jet gas flow method, but is considerably longer than the 4.85×10^{-10} obtained by J. G. Parker, C. E. Adams, and R. M. Stavseth[27]. Parker, Adams, and Stavseth also used equation (2.12), which contains the ratio α_{exp}/α_{cl}, to obtain 4.95×10^{-10} for the rotational relaxation time of oxygen.

E. F. Green and D. F. Hornig[28] obtained rotational collision numbers of 17 for nitrogen and oxygen at 100°C from shock tube measurements. These collision numbers are significantly higher than the room-temperature data of Martin Greenspan's[29] which are 5.26 for oxygen and 4.09 for nitrogen. These collision numbers reported by Greenspan are probably the best values because his instrument was capable of attaining f/p values of approximately 200 MHz/atm, thus observing most of the rotational dispersion region at room temperature. All other acoustical investigations have used the questionable equation (2.12) to calculate the rotational collision numbers.

Experimental Data

Experimental velocity and absorption data are presented below for nitrogen and oxygen. Figs. 15 through 21 show plots of $\alpha_{mol}\lambda$, the measured absorption minus the classical absorption times the wavelength, and the velocity squared versus f/p in MHz/atm. The classical absorption in all of these gases has been calculated using thermodynamic data taken from reference 20 with the high-temperature values obtained by extrapolation. The solid curves for oxygen and nitrogen have been drawn from single-relaxation theory with the relaxation time chosen to fit the absorption data. Gases were used as received from the Linde Air Products Company without further treatment to increase purity.

Oxygen

The oxygen used was reported as 99.5% pure with less than .01% water vapor. Fig. 15 shows a plot of $\alpha_{mol}\lambda$ for oxygen at 23°C. The velocity dispersion is only approximately two meters/sec from .7 to 40

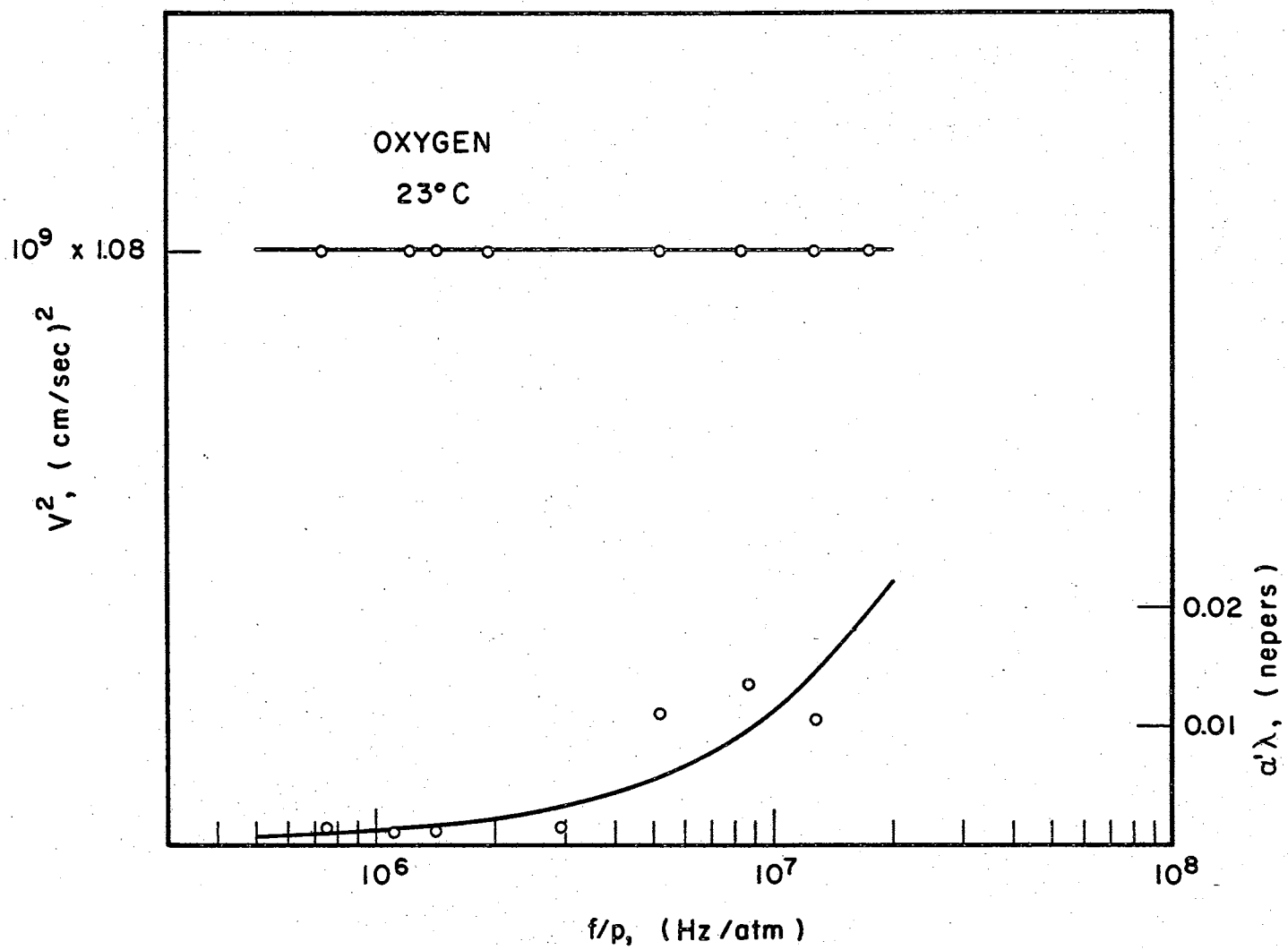

Figure 15. Dispersion and Absorption in Oxygen, 23°C

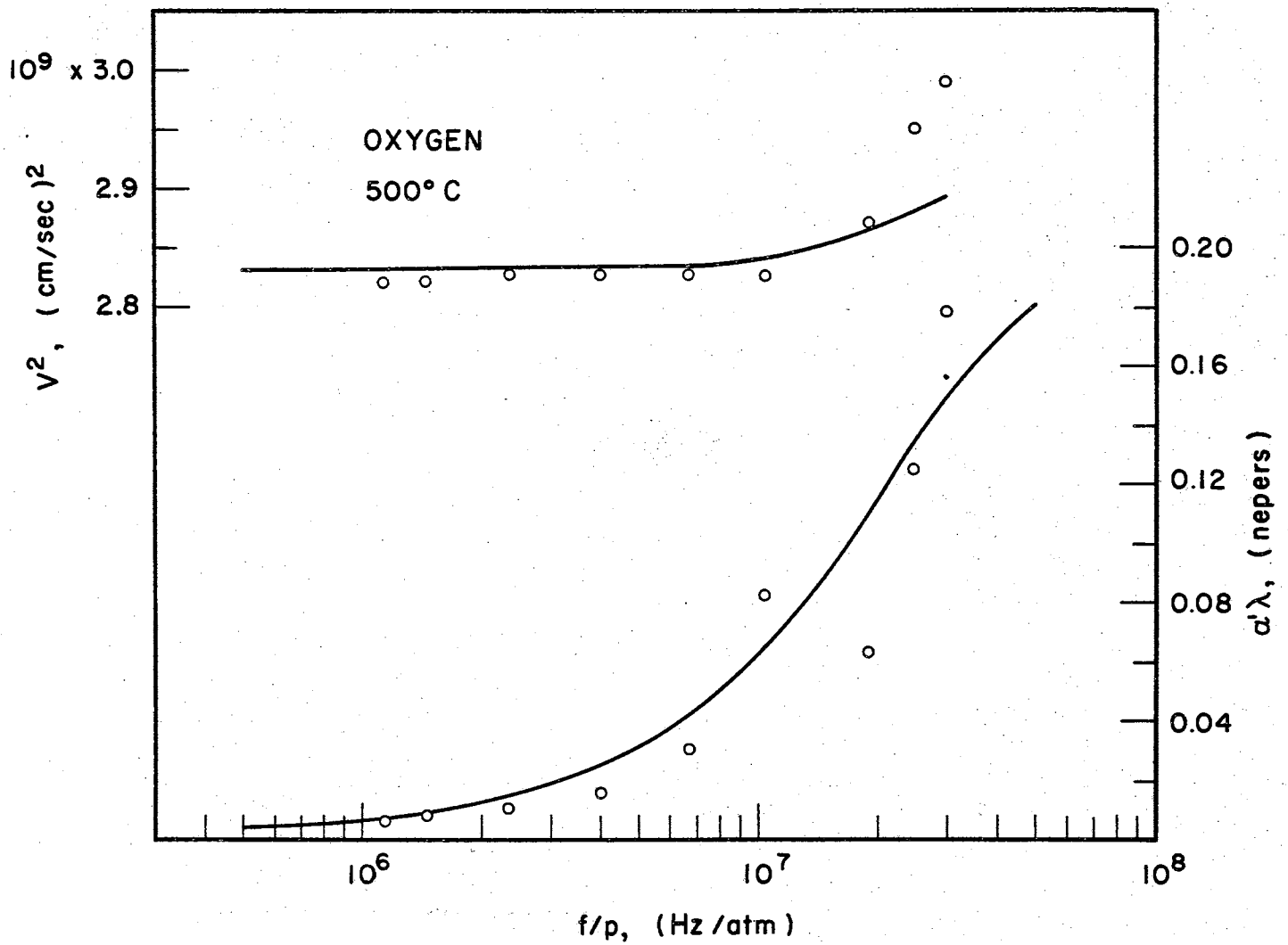

Figure 16. Dispersion and Absorption in Oxygen, 500°C

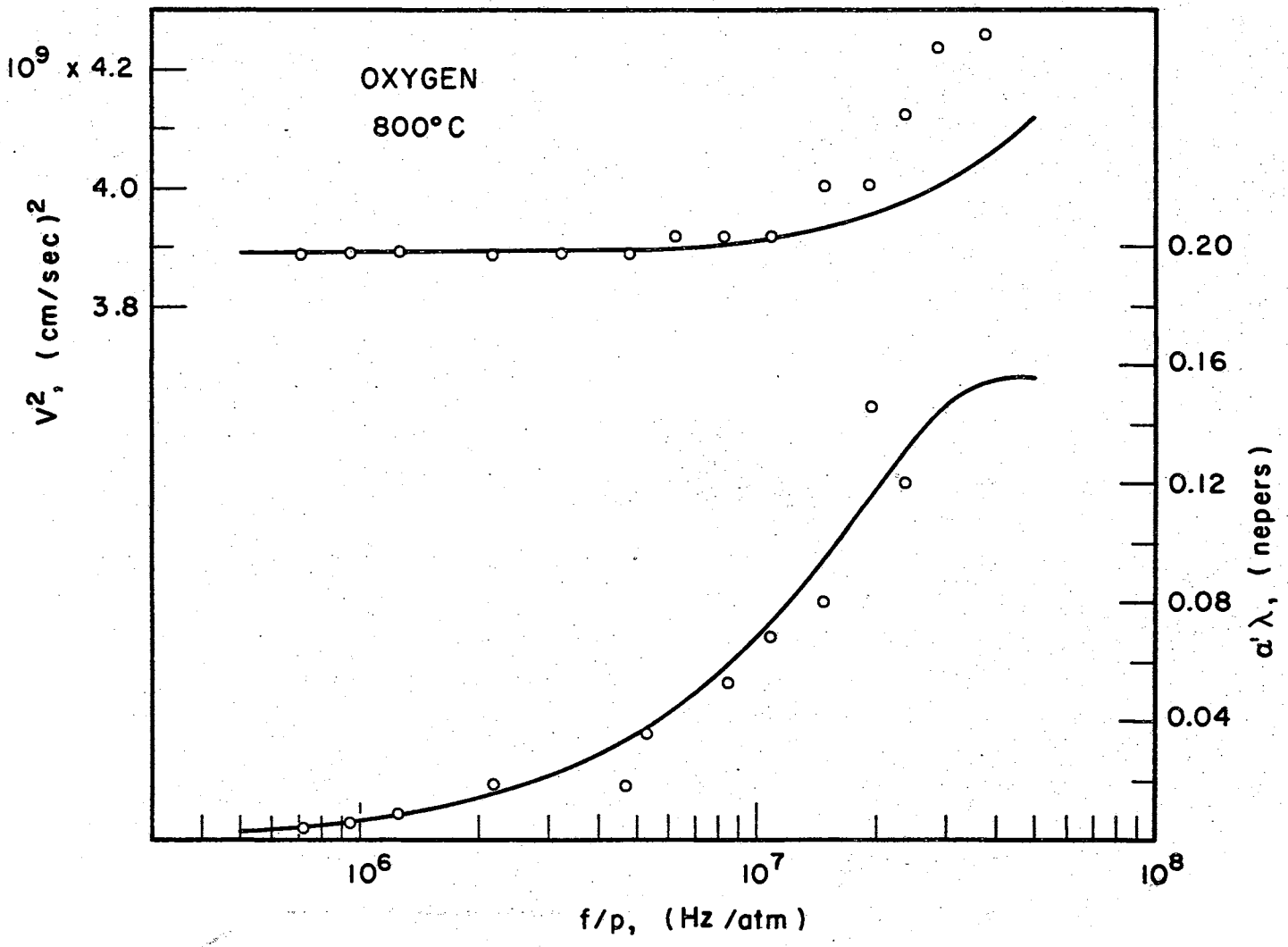

Figure 17. Dispersion and Absorption in Oxygen, 800°C

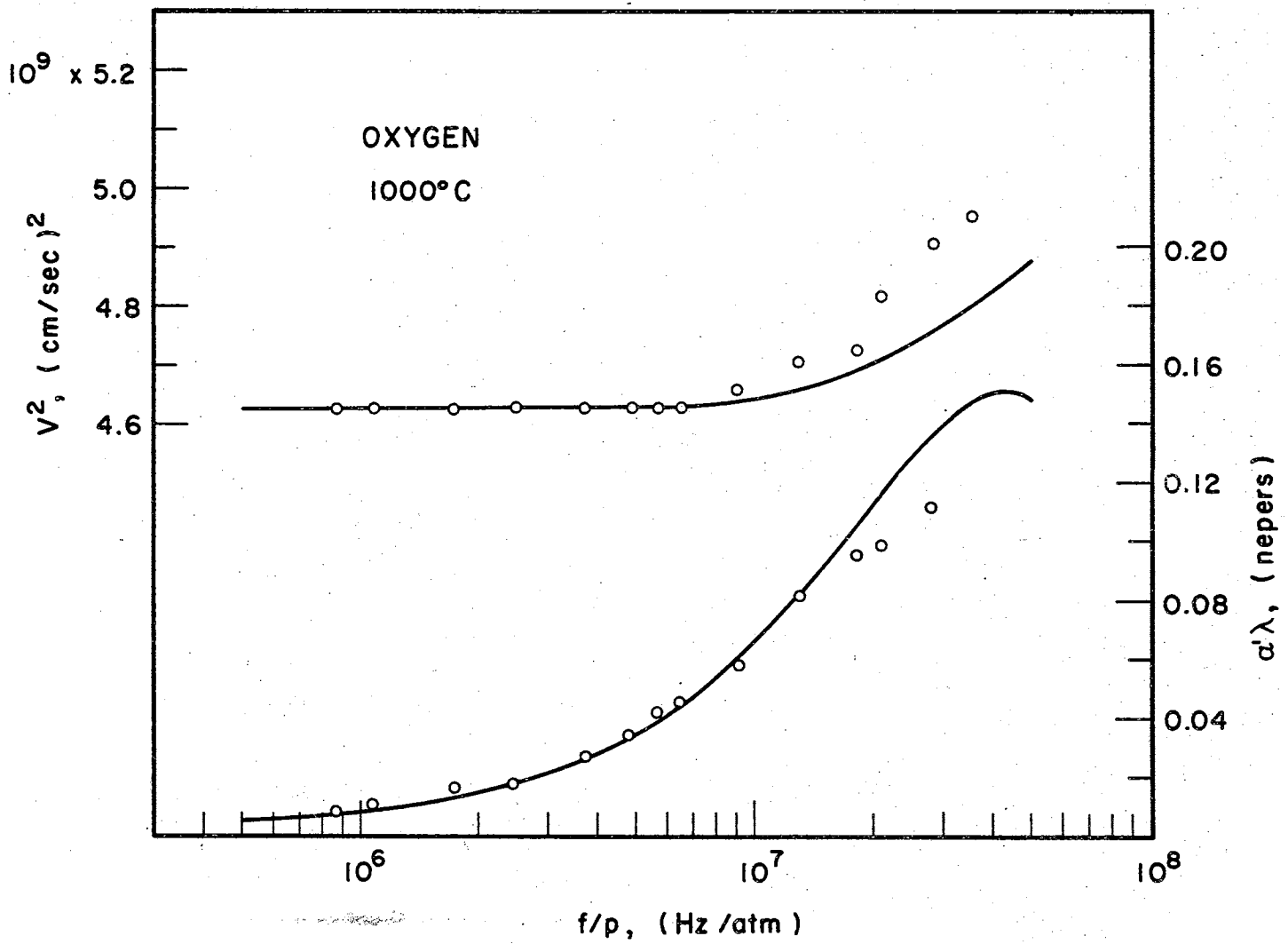

Figure 18. Dispersion and Absorption in Oxygen, 1000°C

MHz/atm. The scatter of the absorption data is large because the peak of the absorption curve is above 300 MHz/atm[30], and consequently, the measured absorption is nearly equal to the classical absorption. Figs. 16, 17, and 18 show oxygen data at 500, 800, and 1000°C. The absorption peak shifts from well beyond the range of the instrument at room temperature to the neighborhood of 45 MHz/atm at 1000°C. The dispersion at high temperature and high f/p is larger than that predicted by single-relaxation theory. For example, at 800°C and 28 MHz/atm the experimental velocity was found to be 654 ± 5 m/sec and the theoretical velocity was calculated to be 641 m/sec. This excess dispersion is not ascribed to either translational relaxation or to measurement error because argon at this temperature showed no detectable dispersion up to 40 MHz/atm. If the actual velocity of the sound in oxygen were on the low side of the probable numerical error in velocity, the velocity would be 654 less 5, or 649 m/sec. A change in velocity of 5 m/sec could also have been detected in argon. Thus, the dispersion of sound in oxygen due to translational dispersion should be less than 5 m/sec. If the translational dispersion is 5 m/sec, this would reduce the experimental value to 644 m/sec in oxygen. Since this is greater than the theoretical value of 641 m/sec and the experimental values are consistently larger than the theoretical values for other high f/p data points, the excess dispersion is probably not due to translational dispersion.

Nitrogen

The nitrogen used was reported by the Linde Air Products Company to have a purity of 99.995%. The room-temperature nitrogen data shown by Fig. 19 corresponds closely to the oxygen data. Previous experiments

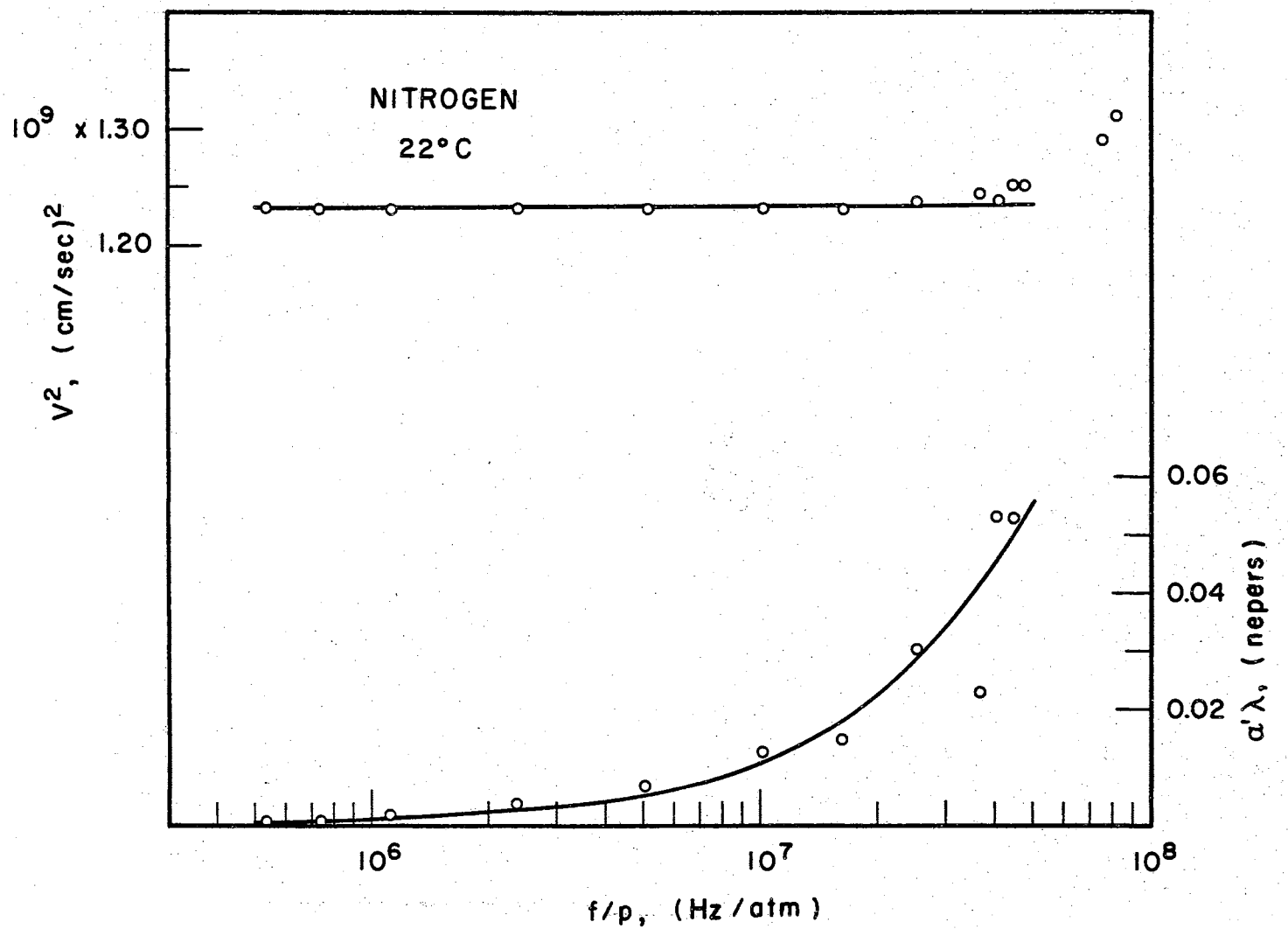

Figure 19. Dispersion and Absorption in Nitrogen, 22°C

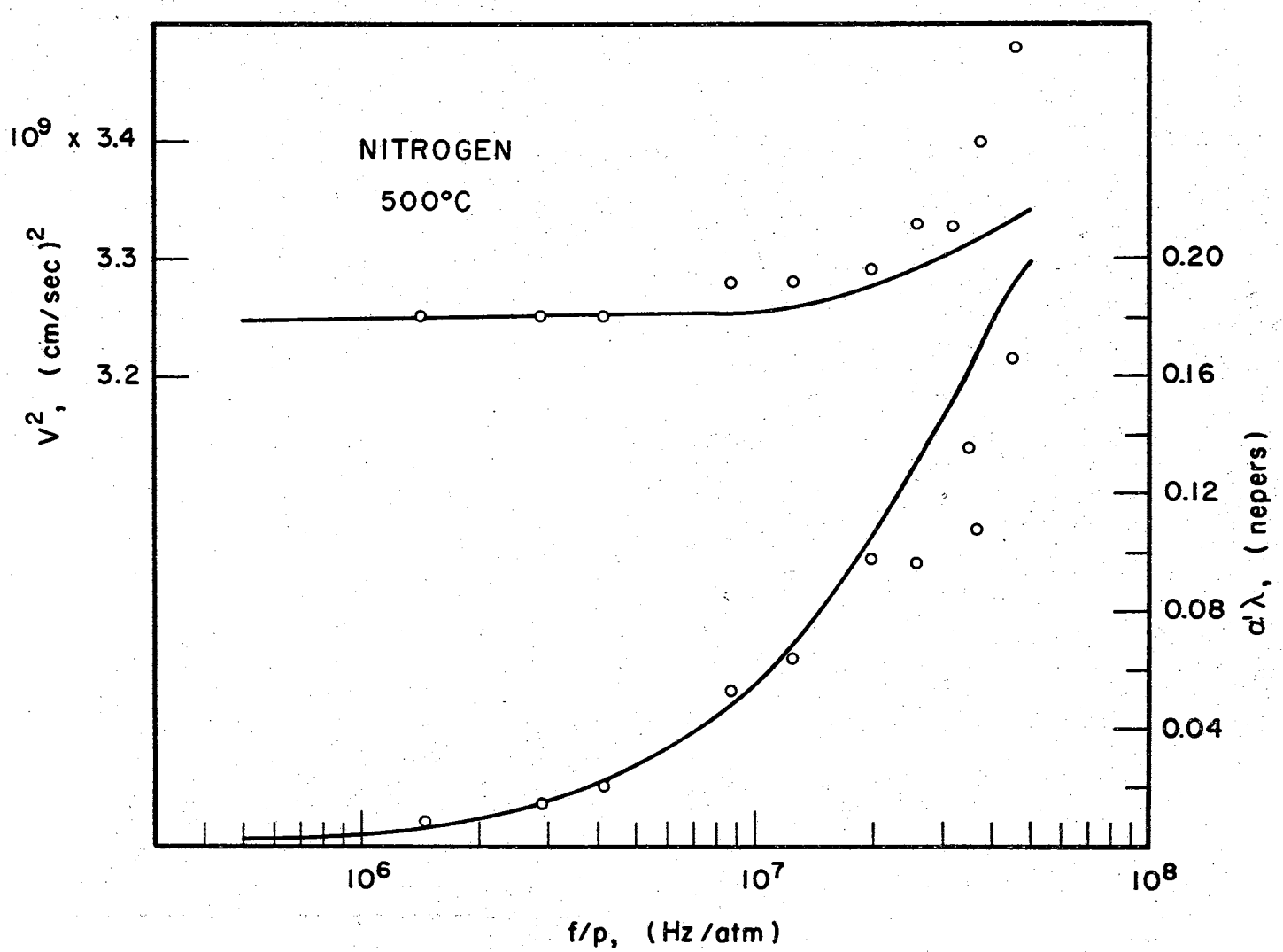

Figure 20. Dispersion and Absorption in Nitrogen, 500°C

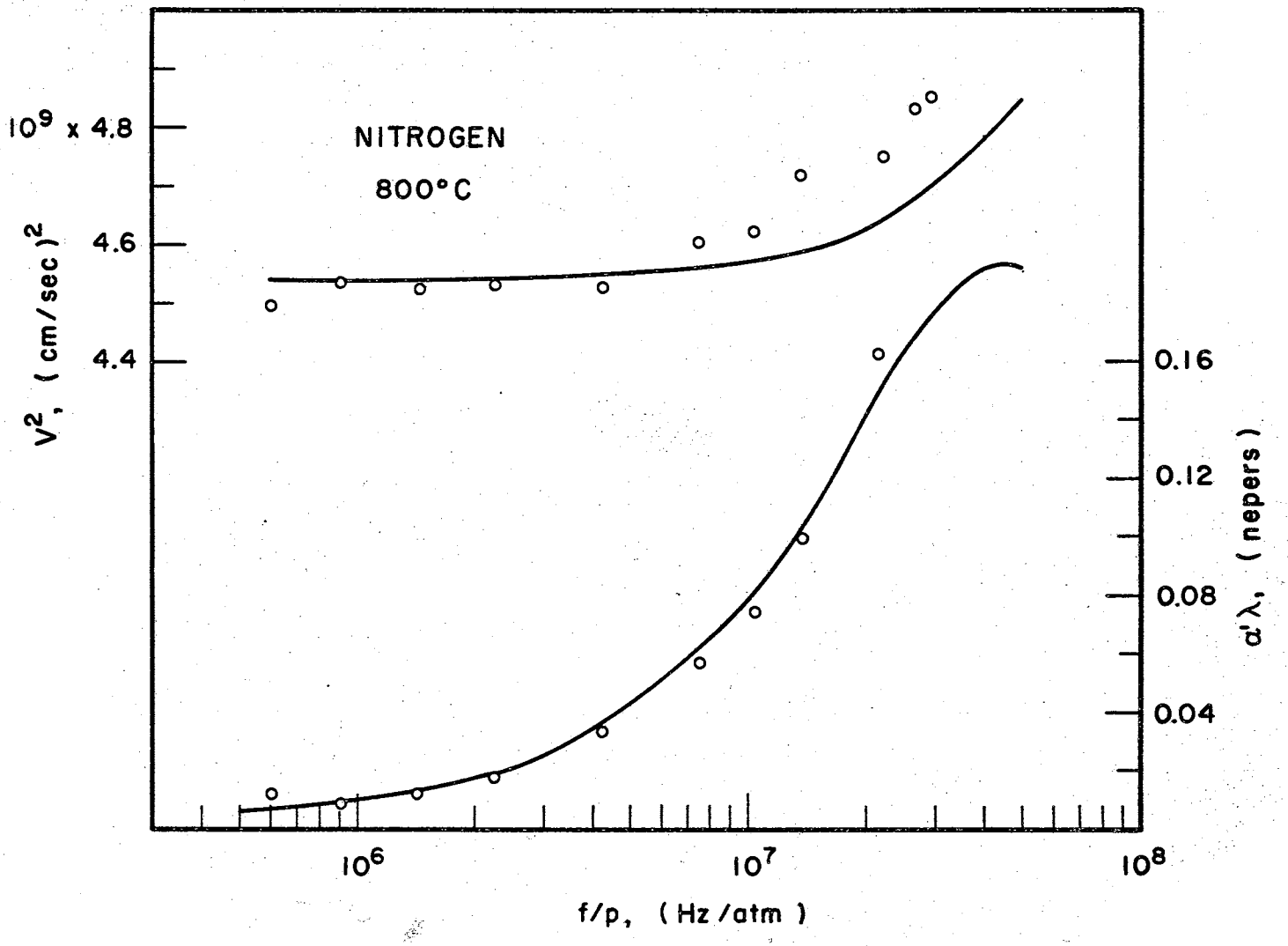

Figure 21. Dispersion and Absorption in Nitrogen, 800°C

locate the absorption peak above 300 MHz/atm[30]. The velocity dispersion in this investigation was found to be 3 m/sec from .7 to 45 MHz/atm. Figs. 20 and 21 show nitrogen data taken at 500 and 800°C. The dispersion in nitrogen at 800°C is 25 m/sec, which is larger than the value predicted by single-relaxation theory. As in oxygen, temperature increases result in a shift of the absorption peak to lower f/p values. Again, the absorption curve shifts from over 300 MHz/atm at 23°C to 50 MHz/atm at 800°C. The relaxation times for nitrogen and oxygen at all temperatures as calculated from best fit of single relaxation theory have been collected in Table I.

Discussion of Nitrogen and Oxygen Results

The velocity dispersion and absorption in oxygen and nitrogen appear quite similar from room temperature to 800°C. At room temperature, the dispersion regions are above the frequency range of the instrument used in this investigation, but other investigations have shown that the dispersion frequency is above 300 MHz/atm. As the temperature increased, the inflection point was found to move to lower frequencies, and in oxygen the dispersion range shifts from over 300 MHz/atm to approximately 45 MHz/atm at 1000°C. This shift in the absorption peak is much larger than that observed in hydrogen or deuterium. In both nitrogen and oxygen, the velocity dispersion at high temperatures and high f/p is larger than that predicted by single-relaxation theory. At high temperatures, the magnitude of velocity dispersion is over 25 m/sec.

TABLE I

SUMMARY OF RELAXATION TIMES AT ONE ATMOSPHERE FOR BEST FIT OF SINGLE RELAXATION THEORY TO EXPERIMENTAL DATA, TOGETHER WITH COLLISION TIMES AND THE RESULTANT COLLISION NUMBERS

	T	τ_{exp}	τ_c	Z_{rot}
	^oK	$(x10^{-8}$ sec)	$(x10^{-10}$ sec)	
	295	1.5	.68	220
H_2	873	4.30	1.42	303
	1073	5.0	1.63	307
	298	1.5	.68	220
$P\text{-}H_2$	573	3	1.06	270
	773	4	1.28	310
	295	1.8	.95	188
D_2	773	4.5 x 10	2.0	225
	1073	7.5	2.29	328
	295	.05[a]	1.38	3.6
N_2	773	.3	2.65	11.3
	1073	.5	3.24	15.4
	295	.038[a]	1.86	2.0
O_2	773	.4	3.1	12.9
	1073	.5	3.88	12.9
	1273	.5	4.32	11.6

[a]From G. Sessler, Acustica 8, 395-397, (1958).

CHAPTER V

SUMMARY OF RESULTS

The purpose of this investigation was to determine the temperature dependence of the rotational relaxation for some diatomic molecules. The rotational relaxation has been investigated for nitrogen, oxygen, deuterium, and two modifications of hydrogen.

The relaxation times at one atmosphere used for best fit of single-relaxation theory to the data of this investigation have been collected in Table I. This table also shows the time between collisions, τ_c, at various temperatures for each gas, calculated from $\tau_c = n/1.271p$ where n is the viscosity and p the pressure in cgs units. The average number of collisons for energy exchange, $Z_{rot} = \tau/\tau_c$, is also given.

This investigation has produced the following discoveries about the rotational relaxation of diatomic molecules: (1) the relaxation time as determined by best fit of single-relaxation theory to the acoustic absorption and dispersion curves increases with increasing temperature, (2) the rate of increase with temperature is greater for molecules with small rotational characteristic temperature, (3) the dispersion is larger than can be accounted for by single-relaxation theory, (4) the absorption peak is larger and broader than is predicted by single-relaxation theory, and (5) the acoustic behavior of normal and para-hydrogen is indistinguishable at high temperature. One may attempt a qualitative understanding of points (1) and (2) with the following observations.

Parker[6] has predicted that the rotational relaxation time should increase with temperature, but he predicts a shift which is considerably smaller than that observed. This is perhaps because Parker calculates the time for the transition from zero rotational energy to kT while the ultrasonic experiment measures the time to shift from one Boltzmann distribution to another distribution which is very close to the first.

Another explanation may be based on the study by Raff[31] which assumed that the relaxation time for a particular transition in hydrogen or deuterium is approximately proportional to the energy gap of the transition and that transitions are thus most probable between adjacent energy levels. He has defined a relaxation time for the transition of n molecules between energy levels i and j as

$$\tau_{ij} = \frac{n\ (E_j - E_i)}{\left\langle \frac{d}{dt}\ (\Delta\epsilon) \right\rangle} \tag{5.1}$$

Since the rate of energy transfer, $\langle d/dt\ (\Delta\epsilon)\rangle$, depends upon n^2, equation (5.1) yields

$$\tau_{ij} \propto \frac{(E_j - E_i)}{p} \tag{5.2}$$

where p is the pressure. The primary reason relaxation times are longer at higher temperatures is that at higher temperatures, rotational energy levels with larger energy gaps are occupied and the transitions between these larger energy gaps result in the longer relaxation times.

In general, as the temperature is increased the population of the higher energy levels increases and these energy levels have larger spacing. An apparent relaxation time, τ', can be defined and associated

with the frequency of maximum absorption and with the inflection frequency, f_o, in the dispersion curve by means of

$$\tau' = \frac{1}{2\pi f_o} \tag{5.3}$$

For a particular temperature, one might consider this apparent relaxation time as being associated with some average ΔE in the ensemble of J states. The most populated level[32] is

$$J_m \approx \left[\frac{T}{2\theta_r}\right]^{\frac{1}{2}} . \tag{5.4}$$

The greatest contribution to the specific heat of the system comes from those J states in the vicinity of J_m so that with the ensemble centered about J_m, a reasonable choice for ΔE is the energy associated with $J_m \rightarrow J_m + 1$.

When a gas is perturbed from a Boltzmann distribution by a sound wave, the return to equilibrium will be determined by the times required for the various transitions, which according to equation (5.2) are proportional to the various ΔE's. The effect of raising the temperature of the gas is to shift the whole distribution to higher J levels and hence, for molecules with small rotational characteristic temperatures, one would expect the low-temperature acoustic behavior to be repeated qualitatively except that the time scale becomes longer. For $\theta_r = 2^oK$ and $T = 800^oK$, there is less than a two-fold increase in ΔE from J = 11 to J = 21. If these spacings were all equal, one would expect behavior similar to a harmonic oscillator which exhibits a single relaxation.

From equation (2.13) the spacing between adjacent energy levels is given by

$$E = 2\theta_r k\ (j + 1). \tag{5.5}$$

By choosing the ΔE associated with J_m to represent the average ΔE and combining equations (5.2), (5.3), (5.4), and (5.5), the apparent relaxation time becomes

$$\tau' \propto \frac{(2\theta_r T)^{\frac{1}{2}}}{p} \tag{5.6}$$

Since the number of collisions per second is proportional to $T^{\frac{1}{2}}$, the above equation implies that the "apparent collision number" will be proportional to $(\theta_r^{\frac{1}{2}} T)$. This increase in energy level spacing may account for an increase in relaxation time with increasing temperature if the rate of energy transfer does not increase to compensate for the larger-spaced energy levels at the higher temperatures. This may also account qualitatively for a longer relaxation time in hydrogen and deuterium than in nitrogen and oxygen.

Fig. 22 is a plot of the apparent relaxation time vs $T^{\frac{1}{2}}$ for the nitrogen and oxygen data contained in Chapter IV. This plot is very insensitive to the temperature exponent and a $T^{1/3}$ plot will fit the data as well as the $T^{\frac{1}{2}}$ plot. Qualitatively the experimental relaxation times agree with a plot of τ' vs $T^{\frac{1}{2}}$. This plot is only qualitative for the following reasons: (1) assumptions used in the derivation of the relationship between τ', θ_r, and T, (2) the absorption data has been approximated by a single-relaxation process, and (3) the relaxation time can not be determined accurately because not all of the absorption curve

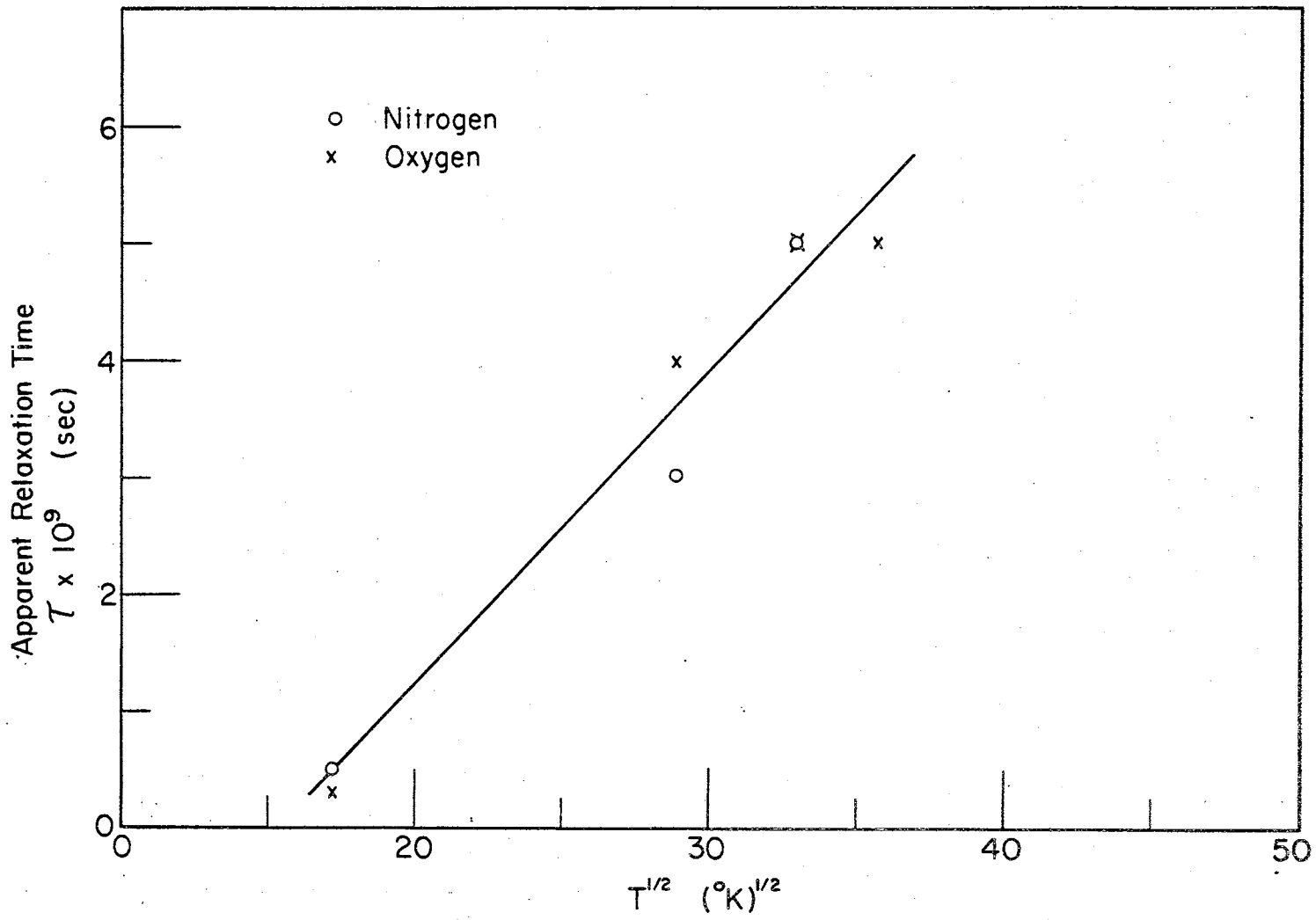

Figure 22. Apparent Relaxation Time Versus Square Root of Temperature

for nitrogen and oxygen can be obtained from the instrument used in this investigation. For reasons (2) and (3) above, considerable uncertainty is introduced into the experimental relaxation time. It is apparent that measurements on several other gases with intermediate characteristic temperatures are needed to check the validity of equation (5.6).

A more rigorous theoretical investigation of the temperature dependence of the rotational relaxation time has been made recently by Raff and Winter[33] which confirms the validity of the general ideas outlined above, but in a manner which attains quantitative agreement with the experimental results presented in Chapters III and IV. The details of these calculations will not be considered here, but a brief description of the investigation and the character of the rate constants obtained is pertinent and will be discussed. Their treatment also includes molecules like hydrogen and deuterium with rotational characteristic temperatures not small enough that the whole ensemble of rotational energy levels can be considered to shift with temperature. They explain in a quantitatively satisfactory manner the variation of the rotational equilibration time with temperature. The rotational systems of hydrogen, deuterium, and nitrogen are represented by a multi-level ensemble. A simple hard sphere collision model is assumed to obtain transition constants. The model contains one adjustable parameter which is fitted to the room-temperature ultrasonic velocity data presented in Chapter III. The velocity dispersion curves are obtained by assuming gaseous ideality and rotational Boltzmann equilibrium at all times.

Individual rate constants, K_{ji}, obtained in the formalism for excitations between levels i and j contain three multiplicative terms which are functions of temperature. (K_{ji} represents the probability per mole-

cule per second that a transition $i \rightarrow j$ will occur.) The excitation rate constants can be reduced to

$$K_{ji} = C_1 N \sqrt{T} \, e^{\frac{-C_2 \Delta E_{ij}}{kT}} \tag{5.7}$$

In this equation, C_1 and C_2 are constants, and N is the concentration of molecules per cubic centimeter. Since the concentration is inversely proportional to the temperature at unit pressure, the excitation rate constants vary as the product of the square root of the absolute temperature, an exponential term containing T, and inversely as the first power of T.

The rate constants such as equation (5.7) are intimately related to the apparent relaxation time. There is a forward and a reverse rate constant for each possible transition, and these rate constants are related by a Boltzmann distribution for near equilibrium conditions. For the two-state case, the relaxation time is the reciprocal of the sum of the forward and reverse rate constants, while for the harmonic oscillator the relaxation time is the reciprocal of the difference of two rate constants. One might expect the apparent relaxation time for a multilevel rotational system to be complicated, but reciprocally related to a function of the population of the individual energy levels and the rate constants associated with the various transitions. There is no theory at present which can relate the apparent relaxation time as defined by equation (5.6) to the rate constants. Raff and Winter have avoided this problem by numerically evaluating the derivative of the rotational temperature with respect to the translational temperature. However, in view of the fact that they have been able to quantitatively

predict the shift of the dispersion to lower frequencies with increasing temperature, their treatment represents the most complete description available which relates the acoustic behavior of rotational relaxation to the rotational energy level spacings and populations. Following are two of their conclusions concerning the rate constants:

1. The origin of the temperature dependence lies in the multi-level character of the model in which transitions between higher J states are always associated with smaller transition constants. At higher temperatures these high J states become more heavily populated, and transitions from them are of greater importance in the over-all equilibration process. Hence, the time scale for the process increases.
2. Since the rotational equilibration process is a multi-level one which cannot be adequately described by a single time-constant, the term "rotational relaxation time" is misleading and should be dropped or used only with great care.

BIBLIOGRAPHY

1. K. F. Herzfeld and T. A. Litovitz, Absorption and Dispersion of Ultrasonic Waves, (Academic Press, New York, 1959).

2. K. Takayanagi, Proc. Phys. Soc. (London) A70, 348 (1957) Sc. Rep. Saitana Univ., A3 (1959).

3. C. S. Wang Chang and G. W. Uhlenbeck, "Transport Phenomena in Polyatomic Gases", Report #CM-681, Project M604-6, U.S. Navy Department, Bureau of Ordnance, Contract #NOrd 7924, Task UMH-3F.

4. K. F. Herzfeld and T. A. Litovitz, Absorption and Dispersion of Ultrasonic Waves, (Academic Press, New York, 1959), Chapter 7.

5. C. G. Berend and S. W. Benson, "Classical Theory of Rotational Relaxation of Diatomic Molecules", to be published.

6. J. G. Parker, Physics of Fluids, 2, 449-462 (1959).

7. L. M. Raff, J. Chem. Phys., 46, 520 (1967) and Erratum Note, J. Chem. Phys., 47, 1884 (1967).

8. T. G. Winter and G. L. Hill, "High Temperature Ultrasonic Measurements of Rotational Relaxation in Hydrogen, Deuterium, Nitrogen, and Oxygen", J. Acoust. Soc. Am., 42, October (1967).

9. K. F. Herzfeld and T. A. Litovitz, Absorption and Dispersion of Ultrasonic Waves, 83, (Academic Press, New York, 1959).

10. T. L. Cottrell and J. C. McCoubrey, Molecular Energy Transfer in Gases, (Butterworths, London, 1961).

11. K. F. Herzfeld and T. A. Litovitz, Absorption and Dispersion of Ultrasonic Waves, 45, (Academic Press, New York, 1959).

12. K. F. Herzfeld and T. A. Litovitz, Absorption and Dispersion of Ultrasonic Waves, 236, (Academic Press, New York, 1959).

13. T. L. Cottrell and J. C. McCoubrey, Molecular Energy Transfer in Gases, 78-84, (Butterworths, London, 1961).

14. A Van Itterbeek and L. Thys, "Measurements on the Absorption and the Velocity of Sound in Hydrogen-, Deuterium-, Helium- and Neon Gas", Physica 9, 889, October (1938).

15. A. S. Roy and M. E. Rose, Proc. Roy. Soc. London, A149, 511 (1935).

16. Ellen S. Steward and James L. Stewart, "Rotational Dispersion in the Velocity, Attenuation, and Reflection of Ultrasonic Waves in Hydrogen and Deuterium", J. Acoust. Soc. Am., 24, no. 2, 194, March (1952).

17. J. Elmer Rhodes, Jr., "The Velocity of Sound in Hydrogen When Rotational Degrees of Freedom Fail to be Excited", Physical Review, 70, nos. 11 and 12, 932, December (1946).

18. K. Geide, "Rotationsrelaxation in Gasformigen Schwefelwasserstaff and Parswasserstaff", Acustica, 13, 37, (1963).

19. C. G. Sluijter, H. F. P. Knaap, J. J. M. Beenakker, Physica, 30, 745-762 (1964).

20. J. Hilsenrath, Tables of Thermodynamic and Transport Properties, (Pergamon Press, Oxford, London, New York, 1960).

21. H. W. Wooley, R. B. Scott, and F. G. Brickwedde, J. Res. Nat. Bur. Stand., 41, 379 (1948).

22. K. F. Herzfeld and T. A. Litovitz, Absorption and Dispersion of Ultrasonic Waves, 134, (Academic Press, New York, 1959).

23. Robert A. Boyer, "Ultrasonic Velocities in Gases at Low Pressures", J. Acoust. Soc. Am., 23, no. 2, 176, March (1951).

24. Alfred Joseph Zmuda, "Dispersion of Velocity and Anamalous Absorption of Ultrasonics in Nitrogen", J. Acoust. Soc. Am., 23, no. 4, 472, July (1951).

25. W. Tempest and H. D. Parbrook, "The Absorption of Sound in Argon, Nitrogen, and Oxygen", Acustica, 7, (1957).

26. Wayland Griffith, "Vibrational Relaxation Times in Gases", J. Applied Phys., 21, 1319, December (1950).

27. J. G. Parker, C. E. Adams, and R. M. Stavseth, "Absorption of Sound in Argon, Nitrogen, and Oxygen at Low Pressures", J. Acoust. Soc. Am., 25, no. 2, 263, March (1953).

28. E. F. Greene and D. F. Hornig, "The Shape and Thickness of Shock Fronts in Argon, Hydrogen, Nitrogen, and Oxygen", J. Chem. Phys., 21, no. 1, 617, April (1953).

29. Martin Greenspan, "Rotational Relaxation in Nitrogen, Oxygen, and Air", J. Acoust. Soc. Am., 31, no. 2, 155, February (1959).

30. G. Sessler, Acustica, 8, 395-397 (1958).

31. L. M. Raff, "Theoretical Investigations of Translation-Rotation

Energy Transfer: (H_2,He) and (D_2,He) Systems", J. Chem. Phys., 46, 520-531, (1967).

32. Warren P. Mason, Physical Acoustics, 192, (Academic Press, New York, 1965).

33. Private Communications.

34. Adalbert Farkas, Orthohydrogen, Parahydrogen and Heavy Hydrogen, (University Press, Cambridge, Eng.) (1935).

35. G. E. Schmauch and A. H. Singleton, "The Ortho-Para Shift of Hydrogen", Cryogenic Engineering News, 42-86, June (1966).

36. G. E. Schmauch and A. H. Singleton, "Ortho- Parahydrogen Conversion", Industrial and Engineering Chemistry, 56, no. 5, 20-31, May (1964).

37. E. R. Grilly, "A Simple Thermal Conductivity Analyzer for Ortho-Para Hydrogen", Review of Scientific Instruments, 24, no. 1, 72-73, January (1953).

APPENDIX A

PREPARATION AND PROCEDURE USED FOR TAKING ULTRASONIC VELOCITY AND ABSORPTION MEASUREMENTS IN GASES

This appendix is designed to describe the instrument used in this investigation and to assist a beginning operator in obtaining ultrasonic velocity and absorption data. Step-by-step instructions on the equipment checkout follow the preliminary comments below. A description is then given of how room-temperature velocity and absorption measurements are obtained, followed by a section outlining the procedure for obtaining this data at high temperatures.

Preliminary Comments

Room-temperature data was taken first, before proceeding to higher temperatures, because room-temperature data exists for most gases and a comparison can be made with the results of other investigators. Also, the operator has the opportunity to familiarize himself with the apparatus before attempting measurements at higher temperatures.

The pressures of the gas were predetermined to permit proper spacing of the data points on the V^2 or $\alpha_{mol}\lambda$ versus $\ln(f/p)$ graph. At low pressures, 10 to 100 mm of Hg, the pressure points were spaced approximately every 5 mm of Hg; at higher pressures, 100 to 1,000 mm of Hg, the pressure spacing was approximately every 100 mm of Hg.

The low-pressure data was taken first, working up to the higher

pressures, i.e., lower f/p values. Exact previously determined pressures were not used, but the flow regulator valve was set to give approximately the desired pressure, allowing it to come to equilibrium. This took approximately one minute. By increasing the flow rate one scale unit, the pressure increased approximately 10 mm of Hg for the next pressure data point.

Data was taken as quickly as possible because of changes in barometric pressure and heating of the rods at high temperature. After completion of the preliminary procedure described below, it took approximately two hours to obtain data at one temperature.

Equipment Checkout

In preparing to take a set of data, the following preliminary steps were completed:

1. All gas lines leading to and from the Vycor tube were checked to be sure they were free from leaks under pressure. This was very important, particularly when measurements were made on an explosive or toxic gas. The gas-handling system is shown in Fig. 23. Note that the valve in the flow meter and valve V_2 control the gas pressure in the Vycor tube inside the tube furnace. A McLeod gage, Kenny Model TD-1, and a manometer were used to measure the pressure over the required range.
2. The Vycor tube and accessory lines were pumped down to 10 microns of Hg with a mechanical vacuum pump.
3. The leak rate on the Vycor tube and accessory lines was checked and found to be .04 mm/hr.
4. The gas regulator was set at about 15-20 p.s.i.g. on the test

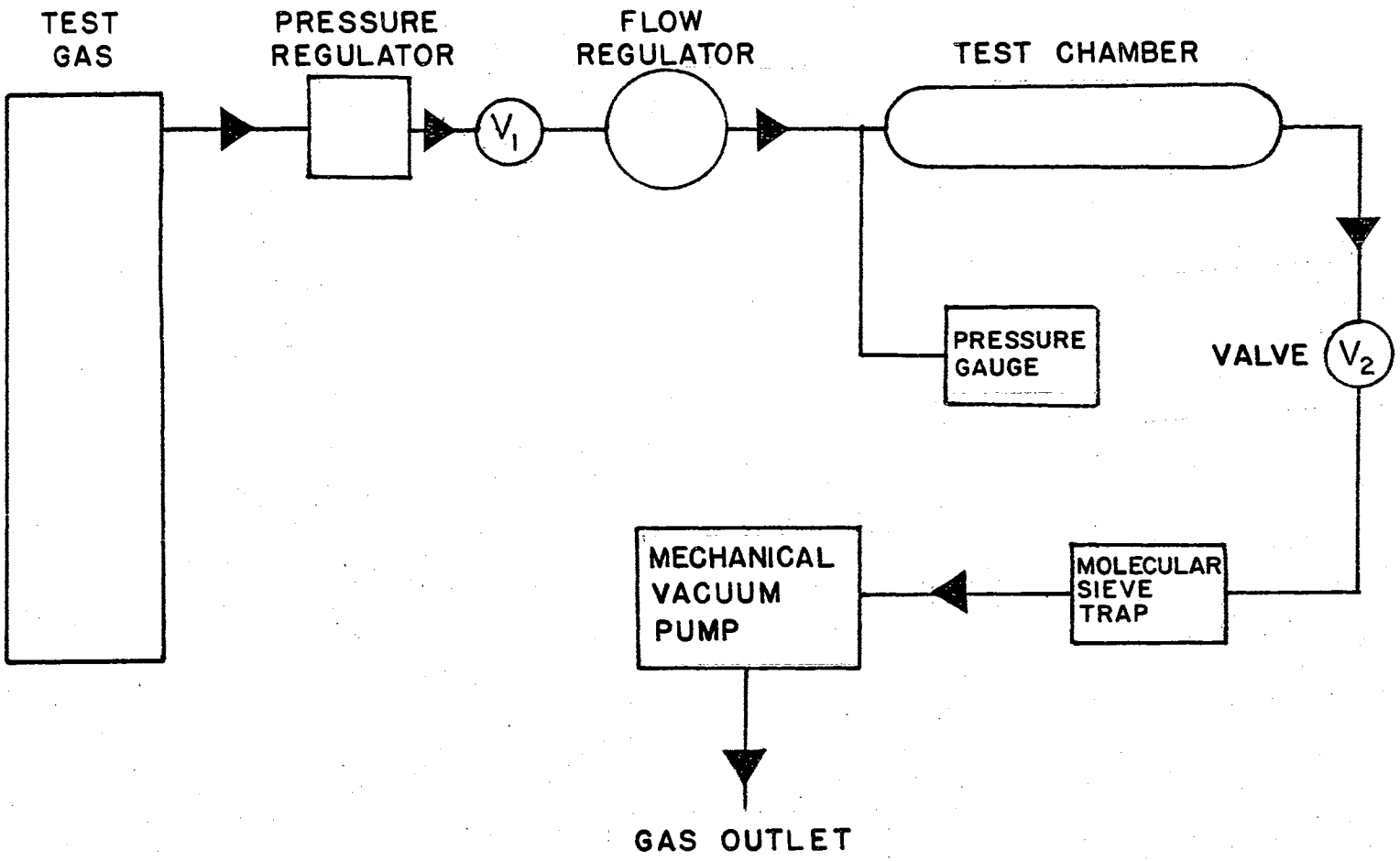

Figure 23. Schematic Drawing of Gas-Handling System

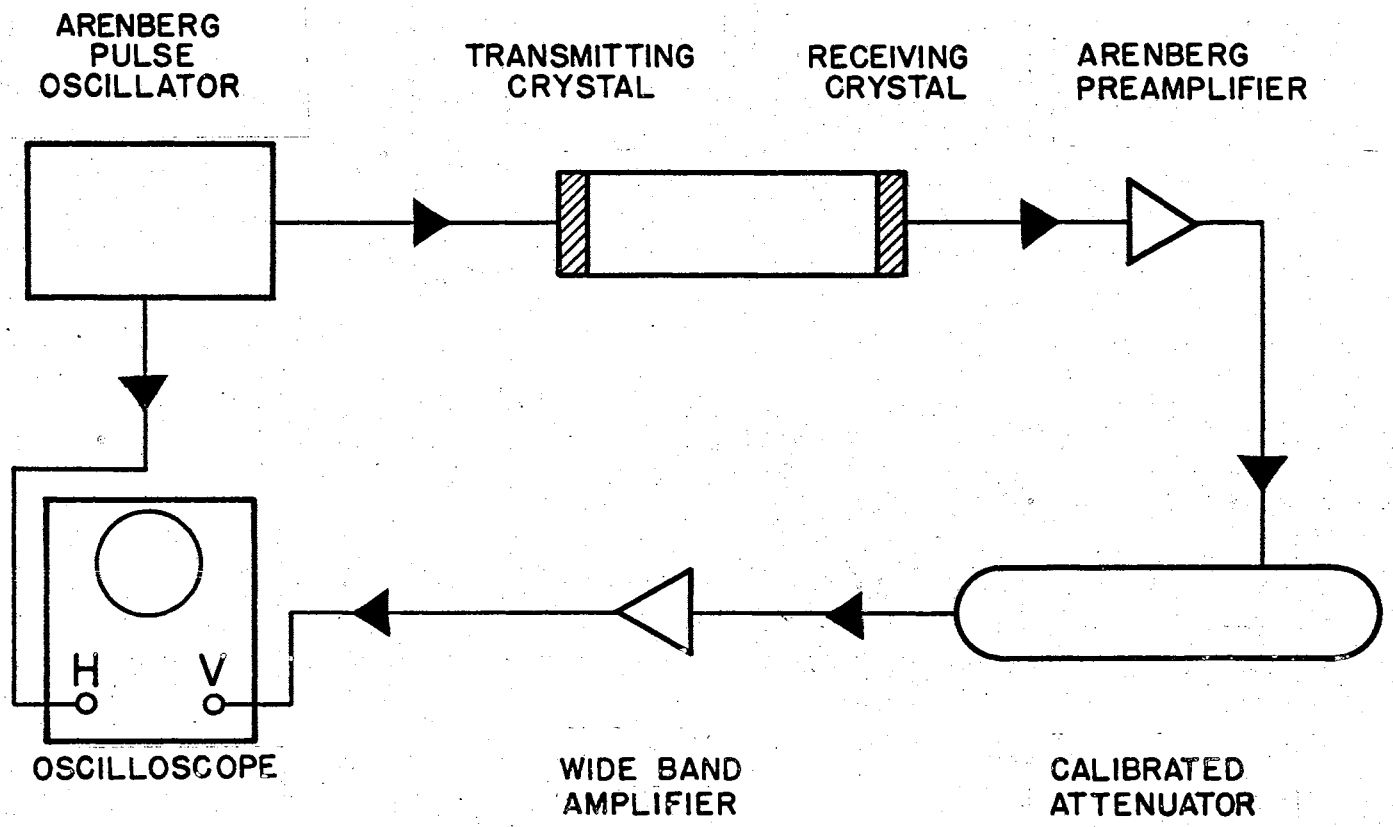

Figure 24. Block Diagram of Electrical Circuit

gas.

5. A gas pressure of 20 mm Hg was put in the Vycor tube chamber to see if the signal strength was normal. When operating properly, there was at least 20 db of signal with a peak-to-peak height of 2 cm on the oscilloscope screen with maximum power output of the pulse oscillator, maximum amplification of the pre-amplifier and wide-band amplifier, and vertical input to the oscilloscope. A low signal intensity occurs when the gain of the pre-amplifier is not on a maximum for input and output or from a bad bond between one of the crystals and its quartz rod (see Appendix B).

6. Fig. 24 is a block diagram of the electrical circuit of the apparatus. An Arenberg Model PG-650C pulse oscillator producing 60 pulses per second with a pulse duration of 22 microseconds excites the crystals and provides a delayed trigger for the horizontal oscilloscope sweep. An Arenberg tuned pre-amplifier, Model PA-620, amplified the signal before it was amplified by a Hewlett Packard wide-band amplifier, Model 460AR. The output from the wide-band amplifier was amplified again by the Hewlett Packard single channel amplifier, Model 1751A. All electrical equipment was allowed to warm up at least 30 minutes before data was attempted. The power switch to the pulse oscillator was turned on at least one minute before the high voltage output switch was turned on. Switch positions of the pulse oscillator were: Trigger - Internal; Delay Time - 1100 microseconds; Pulse Rate Frequency - 60 Hz; R. F. Delay - Out Position; Approximate Vernier Time Delay - 0; High Voltage Out-

put - 100% (maximum). Changeable coil No. 5T (frequency 1.0 to 1.37 MHz) was used.

7. Sometimes troublesome standing wave noise was present in the signal observed on the oscilloscope screen. This was apparent when absorption data was being taken and was caused by radiation from the initial signal of the pulse oscillator. This was eliminated by proper location of the output coax cable leading to the transmitting crystal. When the quartz rods were moved apart at a pressure of 20 mm of Hg, the signal dropped to zero, with only random noise visible. If a megacycle signal was observed when the sound was absorbed (no received signal), then the troublesome inductive radiation coupling was present. This radiation was also recognized from the fact that it did not move in position on the oscilloscope screen as the fused quartz rods were moved apart. The sound signal transmitted through the gas moved when the quartz rod was moved.
8. The variable inductor in the shielded box leading from the output of the pulse oscillator was adjusted until the pulse on the oscilloscope was of maximum height.
9. A cold trap was used to remove condensable vapors from the gas samples. Liquid nitrogen or dry ice and acetone was used as the refrigerant in the cold trap.
10. When the frequency of the pulse oscillator was not known, it was determined by using the method of Lissajous figures. The frequency of the oscillator was always determined after everything was turned to maximum signal strength and the pulse oscillator was on maximum power output. One of the oscilloscope

probes was aircoupled to the variable inductor in the output of the pulse oscillator and attached to the vertical input of the oscilloscope on the ten-volts-per-centimeter scale. Using the other probe, the output from the BC-221-E frequency meter was applied to the horizontal input on the .1 A.C. setting. A two-to-one frequency ratio was used when the pulse oscillator was operating on the third harmonic of the .75 inch lead zirconate transmitting cyrstal. The frequency of the pulse oscillator was 1.065 $\pm$ .005 MHz. A bright spot was observed in the center of the scope screen, with a complex pattern around this center spot. When a frequency exactly two times the pulse oscillator was applied to the horizontal input, the complex pattern became very distinct and stopped rotating. Higher harmonics were also observed, but the Lissajous pattern was more complex. The pattern was always complex because of the pulsed operation.

Velocity and Absorption Measurements

The procedure immediately prior to taking velocity and absorption measurements was to pump the system down to less than .1 mm pressure (determined by the McLeod gage) and determine the barometric pressure using the manometer. The temperature and pressure were recorded, beginning at the lower pressure as described above. It was necessary that this recorded temperature be maintained throughout the data set. One of the highest peaks in the center of the pulse was selected and used for a velocity and for an absorption determination at a given pressure.

In making a velocity measurement, the delayed trigger was adjusted

so that the chosen cycle appeared at the left of the oscilloscope screen. The chosen cycle was centered as nearly as possible on the left vertical line on the grid of the oscilloscope screen. The vernier on the pulse oscillator was used to position the peak approximately correctly. Then the oscilloscope trace adjustment was used for final adjustment. As the rods were moved apart by the micrometer, the path length of the sound increased and the pulse moved from left to right across the oscilloscope screen. When the reference pulse dropped to approximately one cm vertical height, the peak was still clearly visible and the pulse was again centered as nearly as possible on one of the vertical lines of the screen.

The sweep time multiplied by the distance the chosen cycle moved determined the time necessary for the sound to travel the known increase in path length. Thus, the velocity is calculated from the following formula:

$$V = \frac{\text{(distance rod moved in inches) x (2.54 cm/inch)}}{\text{(cm's traveled by reference peak on scope) x (sweep time)}} \quad \text{(I.1)}$$

The sweep time normally used was 2×10^{-6} sec/cm.

When the reference signal moves 10 cm on the oscilloscope, then from equation I.1 the probable percent of error in the velocity equals the probable percent of error in the distance the rod moves (S) plus the probable percent of error in the time (t) required for the sound to travel the distance (S). With the BC-221 frequency meter set on a frequency of 2,000.0 KC and the oscilloscope sweep time on 2 microseconds/cm, there are $40 \pm .1$ waves of the 2 MHz signal in 10 cm on the oscill-

oscope. The percent of error in time is

$$\frac{\Delta t}{t} = \frac{.1\left[\frac{1}{2.0 \times 10^{6}}\right]}{20 \times 10^{-6}} = .25\%$$

The uncertainty due to the instability of the BC-221 frequency meter was .05%. As an example, using the hydrogen data (Fig. 3), the probable percent of error in distance is

$$\frac{\Delta S}{S} = \frac{.002\text{" (uncertainty in micrometer setting)}}{1.241\text{" (distance rod moves)}} \times 100 = .26\%$$

Thus the minimum probable percent of error in velocity in hydrogen at room temperature was approximately .5%. The error in velocity becomes larger than this as the pressure is reduced.

In order to increase the accuracy of the velocity measurements at low pressures, the velocity measurements were made using part of the standing wave region. The error introduced by using the standing wave region was negligible. This could be verified by taking some measurements outside the standing wave region at higher pressure. The reference peak on the scope was always moved across as many cm as possible to reduce the error in velocity measurements to a minimum. It was necessary to remove some attenuation from the attenuator box as the peak moved from the left to the right on the screen.

Absorption measurements were made by separating the rods sufficiently so that standing waves disappeared and then inserting attenuation into the calibrated attenuator until the chosen cycle was 2 cm high. The path length was then increased, decreasing the signal height, and

attenuation was removed from the calibrated attenuator until the signal was again 2 cm high. The absorption in the gas was then determined from the path length and the magnitude of the attenuation. Fig. 25 shows a typical plot of the signal strength in decibels versus the path length. The probable numerical error in an absorption measurement is approximately $\pm$ 1 db because this is the least count of the calibrated attenuator and also because of uncertainty in the signal height of scope readings. Since the total absorption range was 30 db, the minimum probable error was approximately 5% over most of the range of the instrument, with the probable error becoming somewhat larger than 5% at high frequency-to-pressure ratios. See two data points in Fig. 3.

The following considerations were necessary when making absorption measurements:

1. At least 20 db of signal intensity was necessary to give good absorption data with small scatter.
2. At low pressure, the absorption measurements were started as close to the standing wave region as possible; however, the rise and fall of the reference pulse was always less than one decible.
3. The vernier trigger delay of the pulse oscillator must be used to position the signal on the screen. Note that the position of the movable rod and the setting of the trigger delay both determine where the trace of the pulse will appear on the oscilloscope screen.
4. The signal strength versus path difference was always a straight line. At least three intensity points were obtained at each pressure (see Fig. 25).

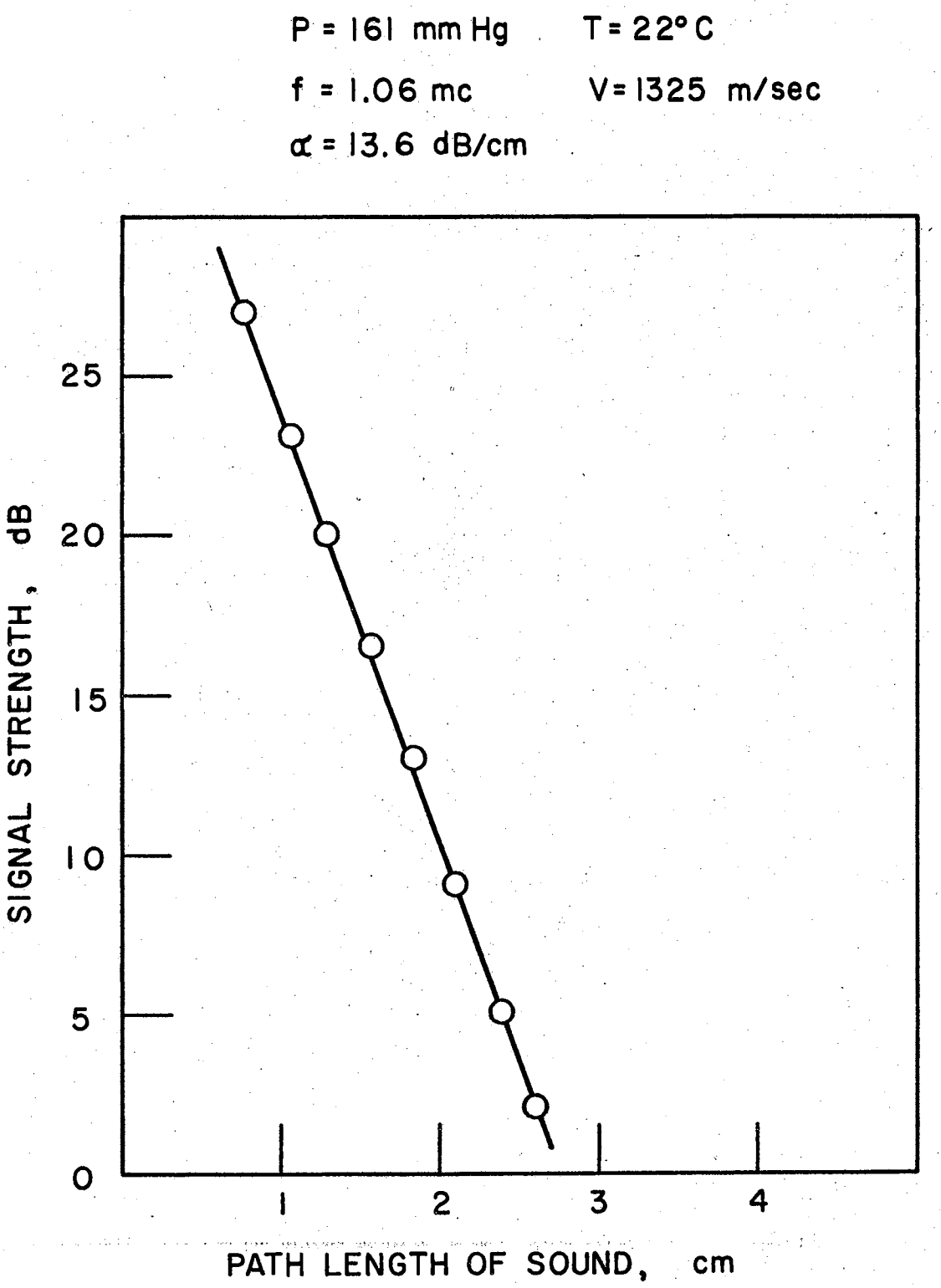

Figure 25. Typical Plot of Signal Strength Versus Path Length of Sound

5. As the signal strength increased at the higher pressures, it was better to use a reference height of 4 cm vertical for the absorption measurements. When the pressure was increased, the signal became stronger than 35 db at a reference height of 4 cm. The envelope of the pulse became non-symmetrical due to the nonlinear amplification of the pre-amplifier. When this happened, the gain of the pre-amplifier was turned down. The gain on the input and output was turned down by the same amount. Any time there was 30 to 35 db of signal strength above the noise the absorption data was very good.
6. When the absorption of sound intensity in the gas was low and the pressure was high, it was necessary to remove the 1-inch spacer in front of the micrometer. This gave a 3-inch sound path and at least 20 db of absorption for most gases.

Procedure for Obtaining Velocity and Absorption Data at High Temperatures

After the room-temperature data was obtained, the preliminary steps discussed above were rechecked to assure that the signal intensity was normal, radiated noise was at a minimum, and the gas-handling system was not leaking. A one-half inch plexiglass shield was placed between the tube furnace and the operator. The barometric pressure was determined using the manometer and recorded. A vacuum was maintained in the Vycor tube until the desired temperature within the tube furnace was reached. This reduced the thermal conduction to the quartz rods.

The water used to cool the outer end of the fused quartz rods and O-rings was started 5 to 10 minutes before heating the tube furnace.

The tap water was cooled with ice for temperature runs above 300°C. The bucket of ice containing the cooling coil was filled every two or three hours. The nitrogen gas used for the inert atmosphere surrounding the tube furnace was also turned on before heating the furnace when measurements were being made on an explosive gas.

The voltage applied to the furnace winding was 115 volts initially, and as the temperature inside the tube furnace neared the desired temperature, the voltage was reduced with an 8.0 amp variac. Approximately 30 volts gave a temperature of 300°C, 50 volts gave 500°C, and 80 volts gave 800°C. The temperature was checked frequently with a Leads and Northrup temperature potentiometer and Chromel Alumel thermocouple. The temperature output was continuous and could be controlled by the variac to within $\pm$ 3°C.

As the temperature within the tube furnace approached that desired, the gas flow was started and the low pressure data was started as described under velocity and absorption measurements. While the pressure was coming to equilibrium, the temperature of the gas was checked and the variac which controls the temperature in the tube furnace was adjusted, if necessary. Also, the signal was returned to the left-hand side of the scope screen so the velocity measurement could be made.

The temperature gradients in the tube furnace were checked closely while the apparatus was under construction. The temperature was constant to within 5°C in the gas and on the inside wall of the Vycor tube over a 3-inch space in the center of the tube furnace for any flow rate of the flow meter. There was a large temperature gradient at the edge of the tube furnace.

APPENDIX B

DISCUSSION, DESIGN, AND ASSEMBLY OF THE ULTRASONIC INSTRUMENT

This appendix contains that information which does not logically fall into the main body of the text. It treats some of the problems encountered during the design and construction of the ultrasonic instrument. One of the major experimental difficulties encountered was the need for maximum power transfer to the transducers and good bonding of the transducers to the fused quartz rods in order to achieve maximum signal strength at low gas pressure. Information on the electrical impedance matching and crystal bonding is followed by detailed instructions for assembling and removing both the stationary and movable quartz rods.

Electrical Impedance

Attention is again called to Fig. 1, which shows the general features of the apparatus frame, quartz rods, quartz rod chucks, and tube furnace. The component electrical equipment and gas-handling equipment have been discussed in Appendix A. Pulsed sine waves were applied to the transmitting crystal through a BNC connector in the quartz rod chuck as shown in Fig. 26. The output impedance of the pulse oscillator was 93 ohms, and in order to transfer a large amount of energy from the oscillator to the transducer, a 93-ohm resistor was used in parallel with a variable inductor and the transmitting crystal. Several T and π imped-

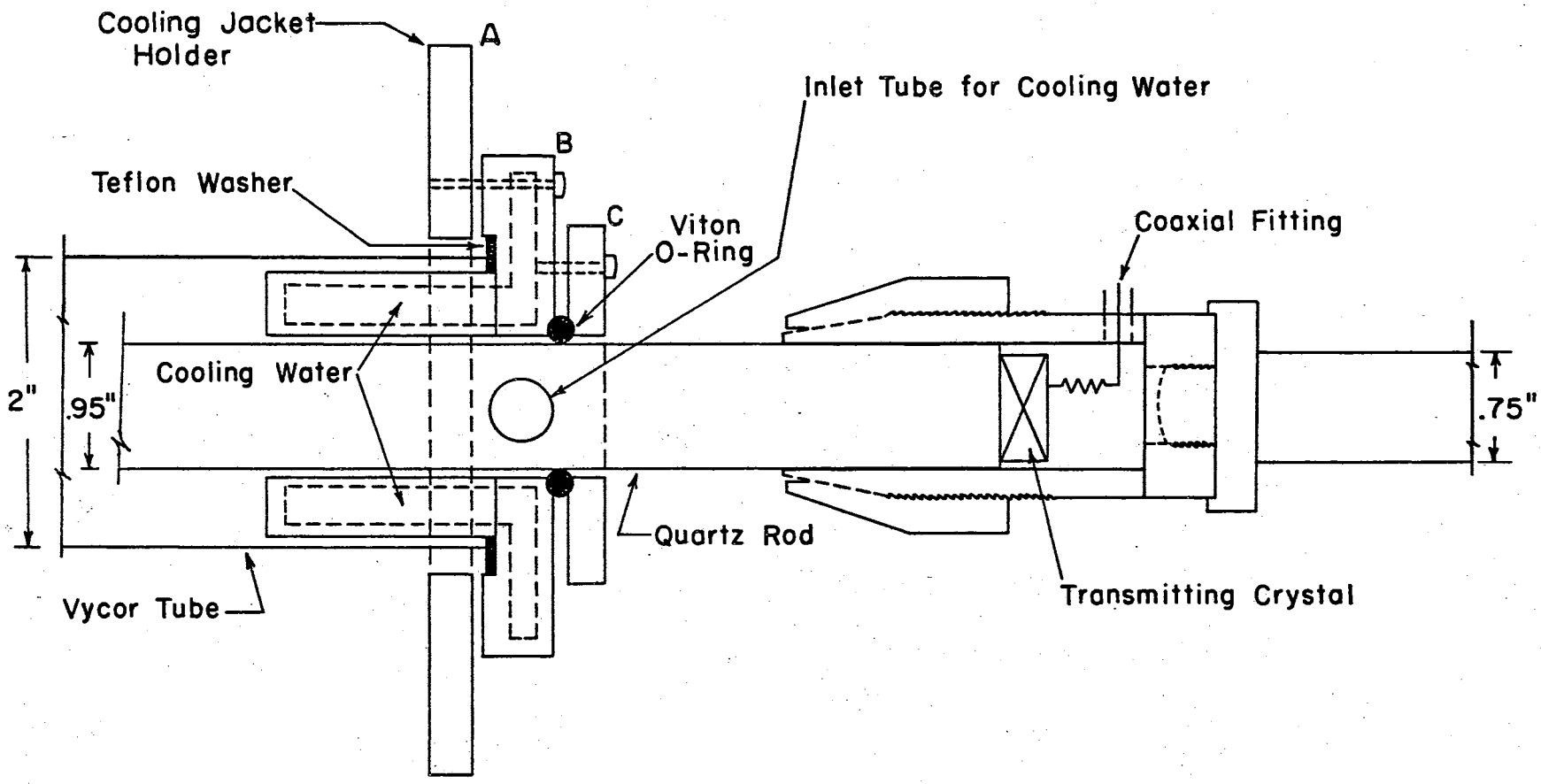

Figure 26. Water-Cooled Vacuum Joint Connecting Vycor Tube and Quartz Rod

ance matching networks and transformers were designed which gave an appropriate impedance for the pulse oscillator. All of these networks created a major problem with radiative coupling to the amplified signal of the receiving transducer, and the signal strength of the apparatus was no larger than that by using the 93-ohm resistor in parallel with the transmitting crystal and variable inductor. The 900-volt peak-to-peak voltage was near the maximum allowable voltage for crystals with a fundamental frequency of 335 kHz. The high-voltage lead to the crystal was a copper spring from the BNC connection to one of the silver faces of the transducer. The ends of the quartz rods were plated with a chromium-gold alloy. The crystal was grounded to the chuck through this chromium-gold plating.

A 200-ohm resistor was also placed in parallel with the wide-band amplifier. This resistor was necessary to provide the 93-ohm output impedance required by the attenuator to give valid absorption data. The oscilloscope was used to check this impedance match, and it was found that an indicated 20 decibles of attenuation would reduce the signal voltage by a factor of 10. A troublesome 60 cycle/sec signal was introduced by the wide-band amplifier and it was necessary to put in a 60 cycle filter to remove this noise before the megacycle signal was amplified by the vertical amplifier of the oscilloscope.

Crystals and Crystal Bonds

The .75-inch diameter crystals have a fundamental frequency of 335 kHz, and were obtained from the Clevite Corporation. The largest f/p range of the instrument was obtained using the third harmonic of 1.065 MHz. The capacitive reactance of the crystals was tuned out with a

series 51 to 102 uh variable inductor as described in Appendix A.

The transmitting crystal was attached to the quartz rod with Aroclor #1260, obtained from the Monsanto Chemical Corporation. Many other types of bonds were tried. Soldering, as well as several other methods of attaching the crystals, initially gave equally strong signals, but the bond always deteriorated after a few minutes of operation at maximum power output from the pulse oscillator. The Aroclor sometimes settled to the bottom of the crystal bond when the apparatus was not used for several weeks. This caused a reduction in signal intensity. In such cases, the crystal was rebonded by removing the quartz rod from the apparatus and placing the rod in a vertical position. A drop of Aroclor was melted on the top of the rod with a heat lamp. The crystal was then placed on top of the rod and a force of two lbs. applied until the Aroclor was cooled (approximately ten minutes). The receiving crystal was bonded by a similar method, using optical wax as the bonding material. This material did not drain from the crystal unless the quartz rod reached a temperature of approximately 100°C.

Assembly and Disassembly of Fused Quartz Rods

The optical grade fused quartz rods used as buffers to transmit the plane sound waves into the tube furnace were obtained from the Valpey Corporation. They were twelve inches long, .950 $\pm$ .005 inch in diameter, with a flatness of 1/10 the wavelength of green light, parallel to 30 seconds of arc or less, perpendicular to 1 minute of arc or less, with optically-polished ends and fine-ground body. These quartz rods were initially aligned coaxially while the tube furnace and Vycor tube were removed from the base of the apparatus. The quartz rods were in-

serted in the chucks and the micrometer adjusted so the outer ends of the rods came together. The rods were adjusted with the alignment screws so the rods were parallel and coaxial. The rods were checked for skewness by placing an eighteen inch metal straight edge on all sides of the rods. A feeler guage showed the ends of the rods were parallel to less than .001 inch. These rods were expensive and difficult to duplicate; therefore, great care was exercised in removing and replacing them. A vacuum was never placed on the Vycor tube unless the chucks were tight, because atmospheric pressure would force the rods together, breaking them. The alignment screws (Fig. 1) were not moved after the initial alignment, and should not be moved unless a complete realignment of the quartz rods becomes necessary.

The following sequence was followed when removing the adjustable quartz rod:

1. One atmosphere of pressure was put in the Vycor tube.
2. The micrometer was positioned to ¼ inch.
3. The chuck was loosened on the rod.
4. Two bolts were removed and the micrometer and micrometer holder removed at the dowel pins, position D, Figs. 1 and 26. The alignment screws were not moved during this process.
5. The O-ring clamp, C, was removed and the quartz rod was slipped from the Vycor tube.
6. Parts A and B, Fig. 26, were then disassembled, if necessary.

Removal of Stationary Quartz Rod

The following sequence was followed when removing the stationary quartz rod:

1. When the plastic inert atmosphere shield was used, it was necessary to partially remove it.
2. One atmosphere of pressure was put in the Vycor tube.
3. The chuck was loosened on the rod.
4. The screws at position E were loosened by ½ inch and the dowel pins positioned so the chuck and holder could be slipped horizontally ½ inch.
5. The chuck and holder were slipped out ½ inch on the horizontal dowel pins.
6. The chuck was tightened and it and the quartz rod were pushed ½ inch toward the furnace.
7. The chuck was then loosened and steps 3 through 6 repeated until the quartz rod was completely free of the chuck.
8. The chuck and chuck holder were removed.
9. The O-ring clamp was loosened and the quartz rod removed.

Replacement of the Stationary Quartz Rod

The following sequence was followed when replacing the stationary quartz rod:

1. The stationary rod was always replaced when the other rod was removed.
2. Dow Corning silicon stopcock grease was placed on the O-ring, teflon washer, and quartz rod near the O-ring position.
3. Parts A', B', and C', Fig. 1, were placed in position, leaving the bolts which hold part A' free to move part A'. The Vycor tube and parts A', B', and C' were centered coaxially in the tube furnace. The rod was slipped through the O-ring, leaving

1¼ inches of the rod outside the O-ring clamp, part C'.

4. The chuck and holder were put into position with dowel pins in place and the bolts at E were tightened.
5. A two-foot long, ½ inch diameter, wooden dowel was placed into the open side of the Vycor tube and used to push the quartz rod approximately one inch into the chuck. Sometimes it was necessary to shift part A' slightly to get the quartz rod to slide into the chuck freely.
6. The chuck was then tightened and the BNC cable attached to the chuck.

Replacement of the Adjustable Quartz Rod

The following sequence was followed when replacing the adjustable quartz rod:

1. The adjustable rod was always replaced after the stationary rod was installed.
2. Dow Corning silicon stopcock grease was placed on the O-ring, teflon washer, and quartz rod near the O-ring position.
3. Parts A, B, and C were placed in position, leaving the bolts which hold part A free to move part A. The Vycor tube and parts A, B, and C were centered coaxially in the tube furnace. The rod was slipped through the O-ring, leaving 1¼ inches of the rod outside the O-ring clamp, part C.
4. The extension in front of the micrometer was removed, and the micrometer placed on the two-inch position.
5. The chuck and chuck holder were bolted into position with the horizontal dowel pins inserted.

6. The quartz rod was slipped into the holder and the chuck tightened.
7. A vacuum was placed on the Vycor tube, the one-inch extension inserted, and the micrometer positioned at zero.
8. The bolts holding parts C and C' in position were then tightened.
9. When the rods were properly aligned, the two springs provided should pull the adjustable quartz rod back three inches from center. The alignment screws were never moved when removing or replacing the quartz rods.
10. The signal strength and vacuum were then checked as discussed in Appendix A.

APPENDIX C

PREPARATION AND ANALYSIS OF PARA-HYDROGEN

Several good references are available which discuss the properties and preparation of para-hydrogen in the liquid state[34-37]. The purpose of this appendix is to discuss the methods used to prepare and analyze small samples of para-hydrogen gas for ultrasonic velocity and absorption measurements. A continuous flow of para-hydrogen was produced by passing normal hydrogen over a catalyst at low temperature. Liquid helium rather than liquid hydrogen was chosen as the coolant because of the hazards associated with liquid hydrogen.

Preparation of Para-Hydrogen

Fig. 27 is a schematic diagram of the equipment used to prepare the para-hydrogen gas. Ultra-high purity hydrogen obtained from the Matheson Company was passed through a flow meter, then into a liquid nitrogen bath where the hydrogen was precooled to liquid nitrogen temperature. The hydrogen then passed into a heat exchanger and over a very effective catalyst. The catalyst, APACHI-I*, was located in a constant temperature bath at 20.5°K. Fig. 28 shows the two innermost glass tubes which act as the heat exchanger and two surrounding glass cylinders. The

*The Linde Air Products Company provided 10 cm^3 of the catalyst APACHI-I. It was activated by flushing twice with high-purity dry nitrogen after heating at 110°C for 24 hrs with a pressure of 10^{-4} torr.

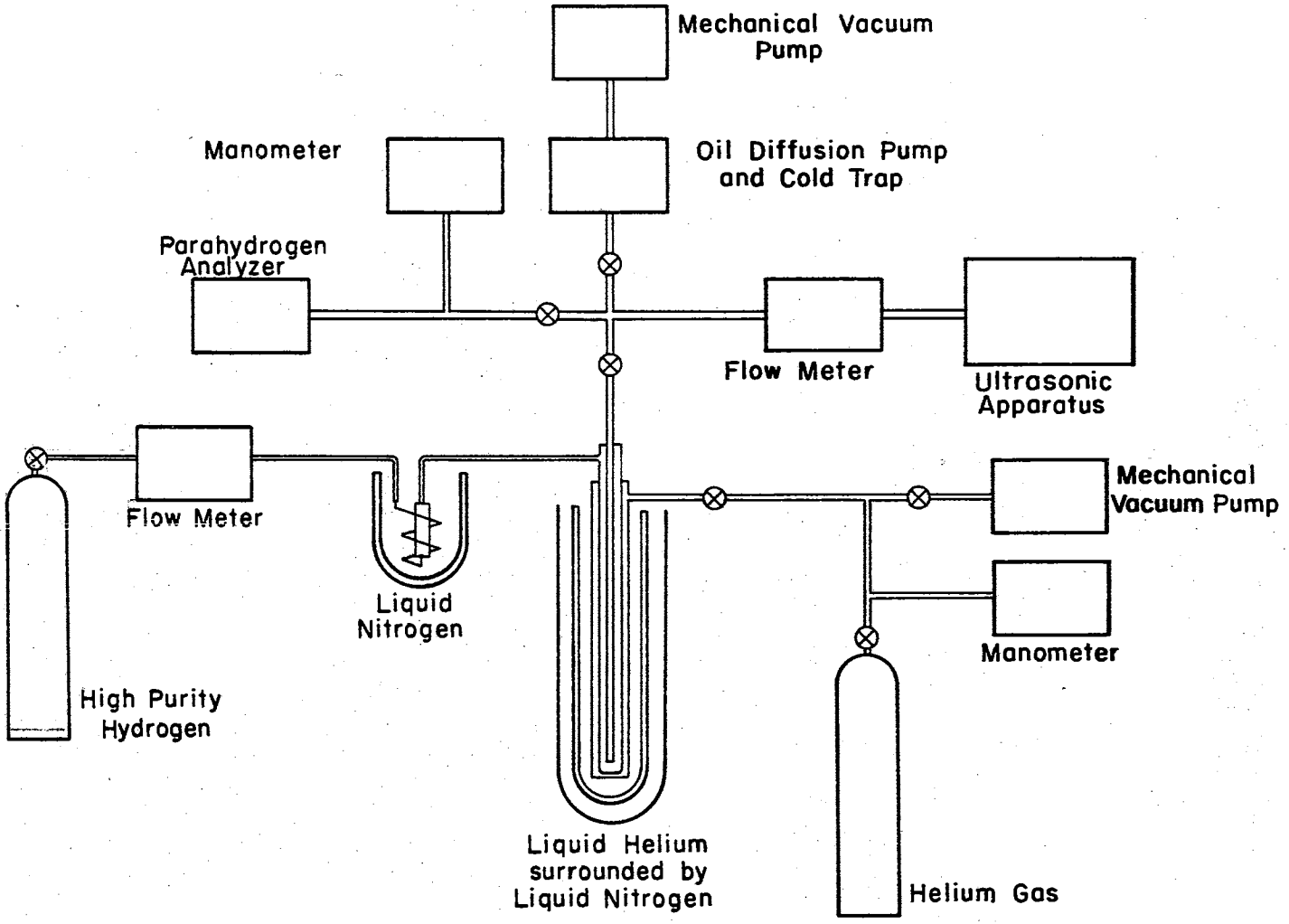

Figure 27. Schematic Drawing of Equipment Used for Preparing Para-Hydrogen

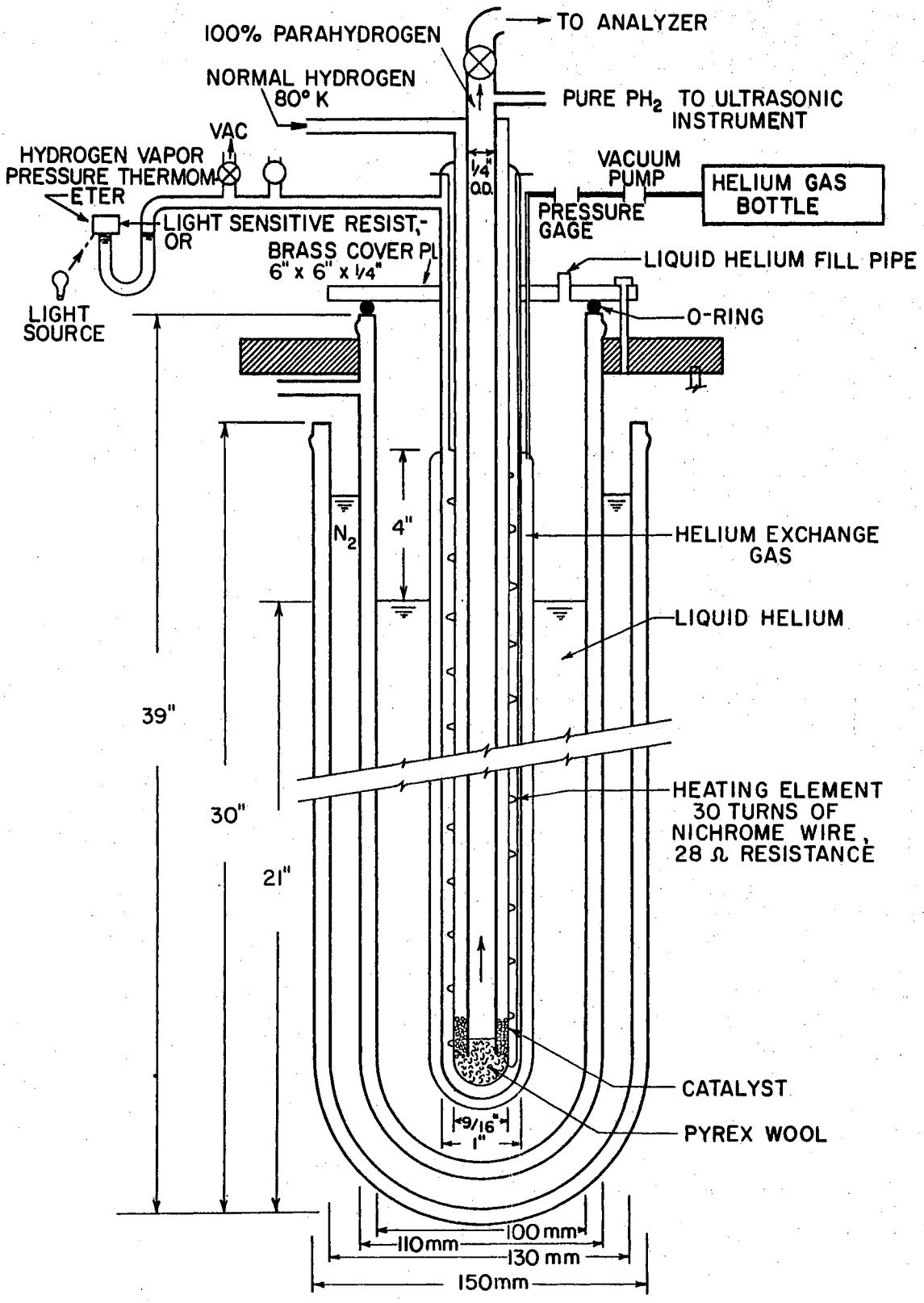

Figure 28. Detailed Drawing of Para-Hydrogen Conversion Chamber

outer cylinder contained a helium exchange gas, and the inner cylinder contained hydrogen gas. The cylindrical hydrogen gas enclosure was essentially a hydrogen vapor pressure thermometer. It was found by experiment that one micron of helium gas pressure would provide an energy exchange which slowly condensed the hydrogen in the hydrogen gas thermometer when hydrogen was flowing through the exchange tubes.

A constant temperature bath for the catalyst was maintained at $20.5^{o}K$, by keeping the vapor pressure of the hydrogen in the surrounding cylinder at 700 mm of Hg. This was accomplished by monitoring the vapor pressure of the hydrogen gas with a manometer. When the vapor pressure dropped below 700 mm of Hg, a nichrome heating element located inside the vapor pressure chamber was turned on by a relay which was activated by a light sensitive resistor acting as a photocell to monitor the mercury level in the manometer. In order to conserve liquid helium the power input to the heating element was reduced to a minimum. Seven volts of potential were applied (approximately one third of the time) to the 30 turns of nichrome wire which had a resistance of 28 ohms.

By using this apparatus, a variable continuous flow of 100% para-hydrogen gas samples was prepared. The flow rates varied from 1 to 10 cubic cm per second. The para-hydrogen gas emerging from the liquid helium dewar could be directed into the analyzer or ultrasonic instrument for velocity and absorption measurements as shown in Fig. 27.

Analysis of Para-Hydrogen

The para-hydrogen content of the gas was analyzed by a thermal conductivity method[37]. The analyzer consisted of two Pirani gages which were resistors in a Wheatstone bridge circuit. The resistance of the

Pirani gages is dependent on the thermal conductivity of the gas within the tubes. The bridge current was first balanced with normal hydrogen at 40 $\pm$ 1 mm of Hg pressure and 79^{o}K in both tubes. Then the variable composition gas to be tested was placed in one tube with normal hydrogen in the other tube. The unbalance bridge current was proportional to the percentage of para-hydrogen[37], and the composition was determined from the deflection of a galvanometer in the Wheatstone bridge. A para-hydrogen change from 25 to 100% produced a difference of only 5 millivolt potential in the bridge circuit. Consequently, in order to detect the para-hydrogen, a Leeds and Northrup D-C galvanometer (#2430, current sensitivity .00045 microamp per millimeter, 502 ohms) in series with a 92.5 K ohm resistor was used in the Wheatstone bridge.

Fifty percent para-hydrogen was prepared by filling the helium exchange tube with liquid nitrogen. After the catalyst had been activated, flow rates in excess of 500 cubic cm per second were not completely converted to 50% para-hydrogen. For the usable flow rates of the ultrasonic instrument (1 to 10 cubic cm per second), the conversion was complete. The deflection of the galvanometer for 100% para-hydrogen was checked with the deflection of the galvanometer when 100% para-hydrogen gas was boiled from equilibrium liquid hydrogen.

VITA

Garnett Lee Hill

Candidate for the Degree of

Doctor of Philosophy

Thesis: HIGH-TEMPERATURE ULTRASONIC MEASUREMENTS OF ROTATIONAL RELAXATION IN DIATOMIC MOLECULES

Major Field: Physics

Biographical:

Personal Data: Born at Tribune, Kansas, July 19, 1935, the son of Anson W. and Catherine S. Hill.

Education: Graduated from Hazelton High School, Hazelton, Kansas, in 1953; received the Bachelor of Science degree from Northwestern State College, Alva, Oklahoma, in May, 1960, with majors in Physics and Mathematics; received the Master of Science degree from the University of Wichita, Wichita, Kansas, in June, 1962, with a major in Physics; completed requirements for the Doctor of Philosophy degree in May, 1968.

Professional experience: Digital Computer Programmer at The Boeing Company from June, 1962, to September, 1963; Physics Instructor at the University of Wichita from September, 1963, to June, 1964.

Other: Student member of the Acoustical Society of America; co-author of a paper entitled "High Temperature Ultrasonic Measurements of Rotational Relaxation in Hydrogen, Deuterium, Nitrogen, and Oxygen", published in the Journal of the Acoustical Society of America, October, 1967; co-author of a second paper on vibrational relaxation times in organic molecules, to be submitted for publication in the near future.